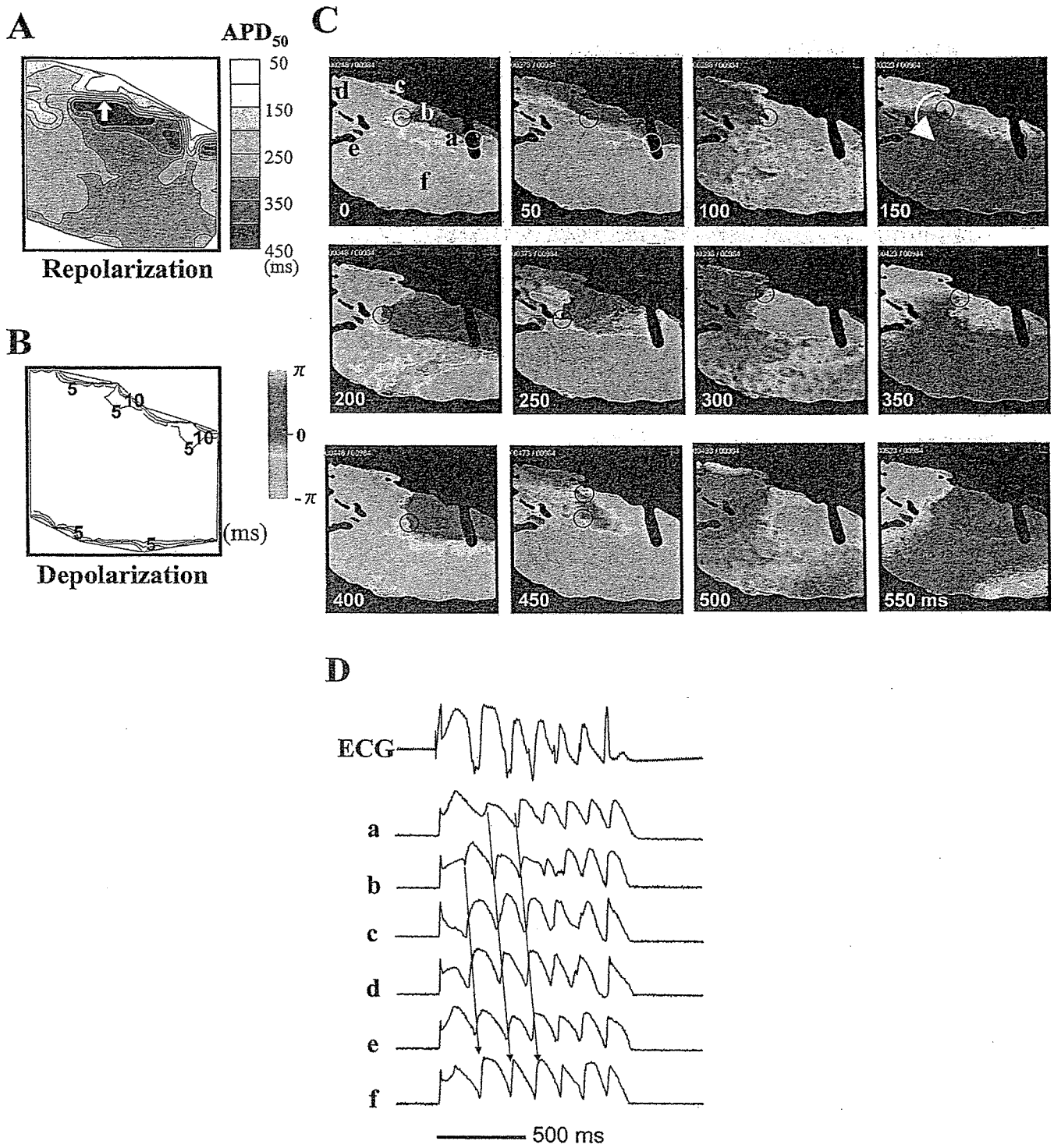

Figure 6. Representative repolarization and depolarization maps on the epicardial surface in the ST-segment elevation (Brugada-ECG) condition just before non-sustained polymorphic ventricular tachycardia (VT) (**A, B**), snapshots of phase movie during polymorphic VT originated from the epicardial phase 2 re-entry (**C**), and optical action potentials at each site (**a to f**) together with a transmural electrocardiogram (ECG) (**D**). **Open circles** = singularity points. APD_{50} = action potential duration at 50% repolarization. Please see the Appendix for accompanying video.

JACC Vol. 47, No. 10, 2006
May 16, 2006:2074–85

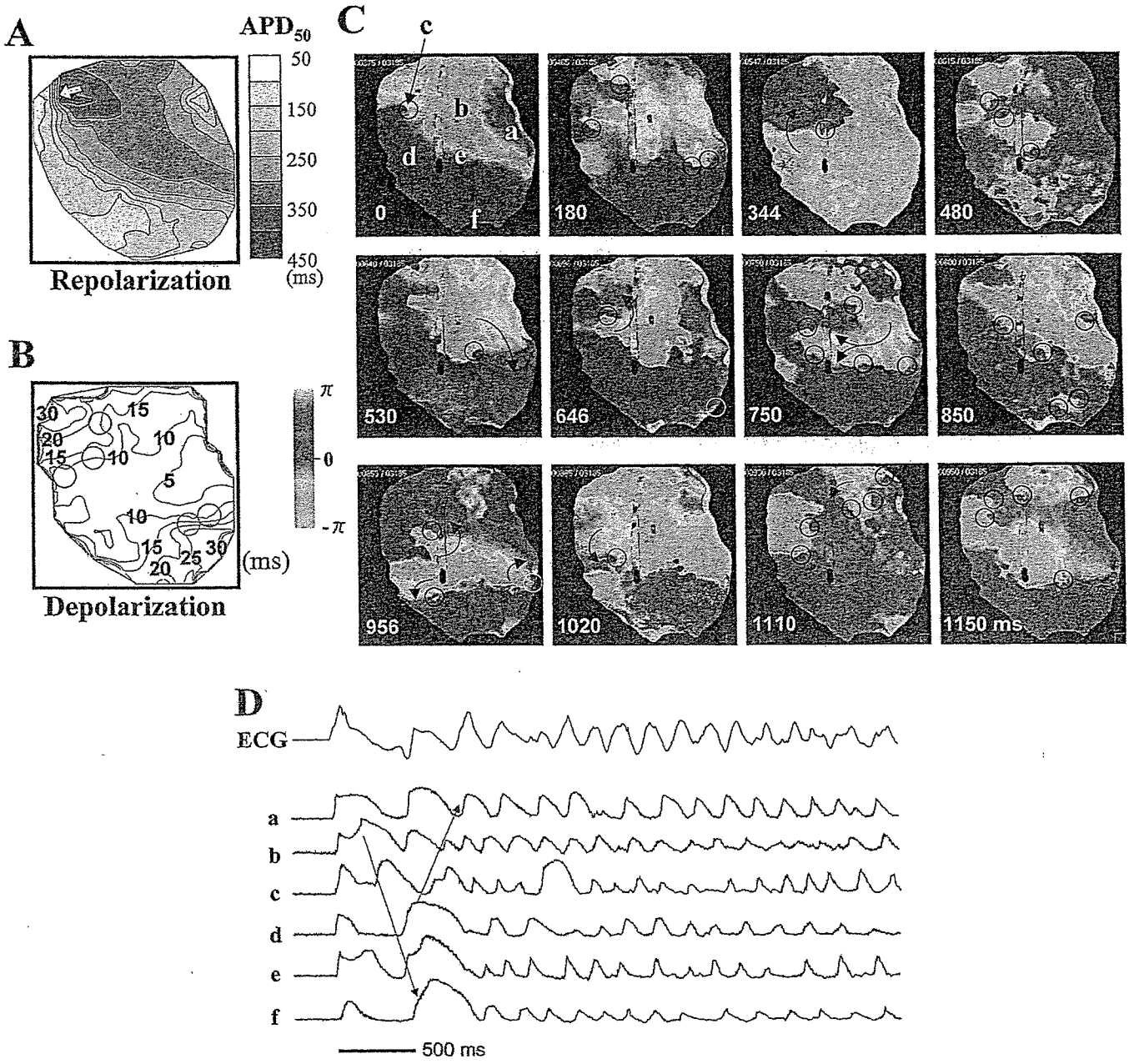

Figure 7. Representative repolarization and depolarization maps on the epicardial surface in the ST-segment elevation (Brugada-ECG) condition just before ventricular fibrillation (VF) **(A, B)**, snapshots of phase movie during VF originated from the epicardial phase 2 re-entry **(C)**, and optical action potentials at each site **(a to f)** together with a transmural electrocardiogram (ECG) **(D)**. **Open circles** = singularity points. APD_{50} = action potential duration at 50% repolarization. Please see the Appendix for accompanying videos.

supports our data that most of P2R-extrasystoles were developed from a small area (<0.5 cm) of GR_{max}.

Maintenance of VF. The only gene linked to the Brugada syndrome is cardiac sodium channel gene, *SCN5A* (17,27). Moreover, sodium channel blockades often unmask Brugada-phenotype, because a loss of sodium channels function enhances both repolarization and depolarization abnormalities (25,28,29). Our experimental study used a pure sodium channel blocker, pilsicainide, to produce the Brugada-ECG associated with prolonged QRS duration and conduction parameters; however, in the Brugada-ECG condition, the depolarization parameters were not different in beats with and without P2R-extrasystoles. In contrast, slower conduction was closely associated with VF susceptibility. These findings suggest that depolarization disturbance was not directly associated with the development of P2R-extrasystole, a trigger of VF, but might contribute to the maintenance of VF in the Brugada-ECG condition.

Electrophysiologic mechanism of VF in the Brugada syndrome has been considered to be re-entry because of high inducibility and reproducibility of VT/VF by pro-

Table 2. ECG, Optical Repolarization, and Depolarization Parameters Just Before Polymorphic VT or VF in the Brugada-ECG Condition

	PVT (n = 12)	VF (n = 5)	p Value
VT/VF CL (ms)	325 ± 33	190 ± 23	<0.001
QRS duration (ms)	74 ± 18	102 ± 23	0.009
J-point (mV)	0.48 ± 0.31	0.43 ± 0.15	NS
Epi max-min APD_{50} (ms)	394 ± 79	344 ± 88	NS
Epi GR_{max} (ms/mm)	169 ± 55	157 ± 22	NS
Sti-Epi interval (ms)	43 ± 10	60 ± 16	0.03
Delta-Epi interval (ms)	13 ± 3	41 ± 16	0.001

Values are mean ± SD.
CL = averaged tachycardia cycle length; PVT = polymorphic ventricular tachycardia; VF = ventricular fibrillation; VT = ventricular tachycardia; other abbreviations as in Table 1.

grammed electrophysiologic stimulation (3,6,14,30), although it is still unclear how VF re-entry is maintained in the Brugada syndrome. In this study, most of the polymorphic VT was single or figure-of-eight type re-entry with no wave-break and terminated within a few seconds (Fig. 6C). In contrast, wave-break in VF group occurred during the first re-entrant wave and took place at sites of the delayed epicardial conduction (Fig. 7B). Wu et al. (31) demonstrated that Ca^{2+} and fast Na^+ current inhibition turned fast VF into slow VF by flattering APD restitution and increasing conduction time. In this Brugada model, however, VF was characterized as the shorter cycle length and multiple wandering wavelets (Fig. 7C) in spite of the slower conduction (Fig. 8), because APD restitution was not flat but rather an "inverse" pattern (Fig. 9), thus increasing dispersion of repolarization during tachycardia. Krishnan and Antzelevitch (25) had demonstrated the incremental arrhythmogenesis of Na^+ channel dysfunction in the RV epicardium during tachycardia. Flecainide also rate-dependently slowed down the conduction velocity. Thus, fast Na^+ current inhibition strongly enhances both heterogeneity of repolarization and conduction slowing during tachycardia in the Brugada-ECG model, which can easily break up the spiral re-entry, thus degenerating polymorphic VT into VF with multiple wavelets.

Clinical implication. Previous clinical study suggested that induction of VF by programmed ventricular stimulation depended on the severity of depolarization abnormalities such as a longer QRS duration or His-ventricular interval but did not predict the recurrence of cardiac events in symptomatic Brugada syndrome (14,15). Moreover, depolarization and repolarization abnormalities in this syndrome are now considered to be closely correlated (16,29,32,33), supporting our data that both repolarization and depolar-

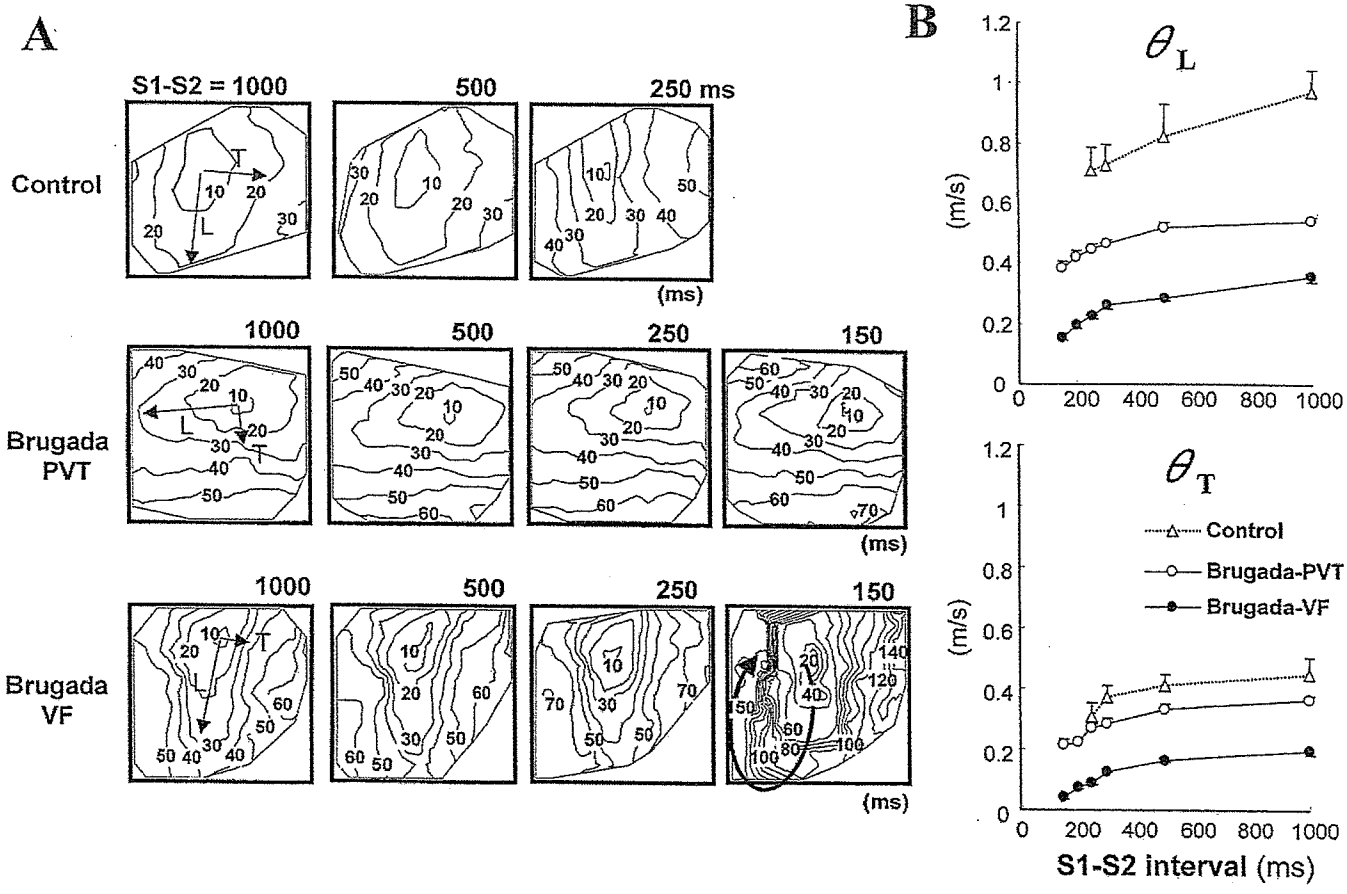

Figure 8. Representative epicardial depolarization maps paced from the epicardium by S1-S2 method in the control and ST-segment elevation (Brugada-ECG) condition with polymorphic ventricular tachycardia (PVT) or ventricular fibrillation (VF) **(A)**, and longitudinal (L) and transverse (T) conduction velocity (θ) restitution curves in each condition **(B)**. Values are mean ± SEM.

JACC Vol. 47, No. 10, 2006
May 16, 2006:2074–85

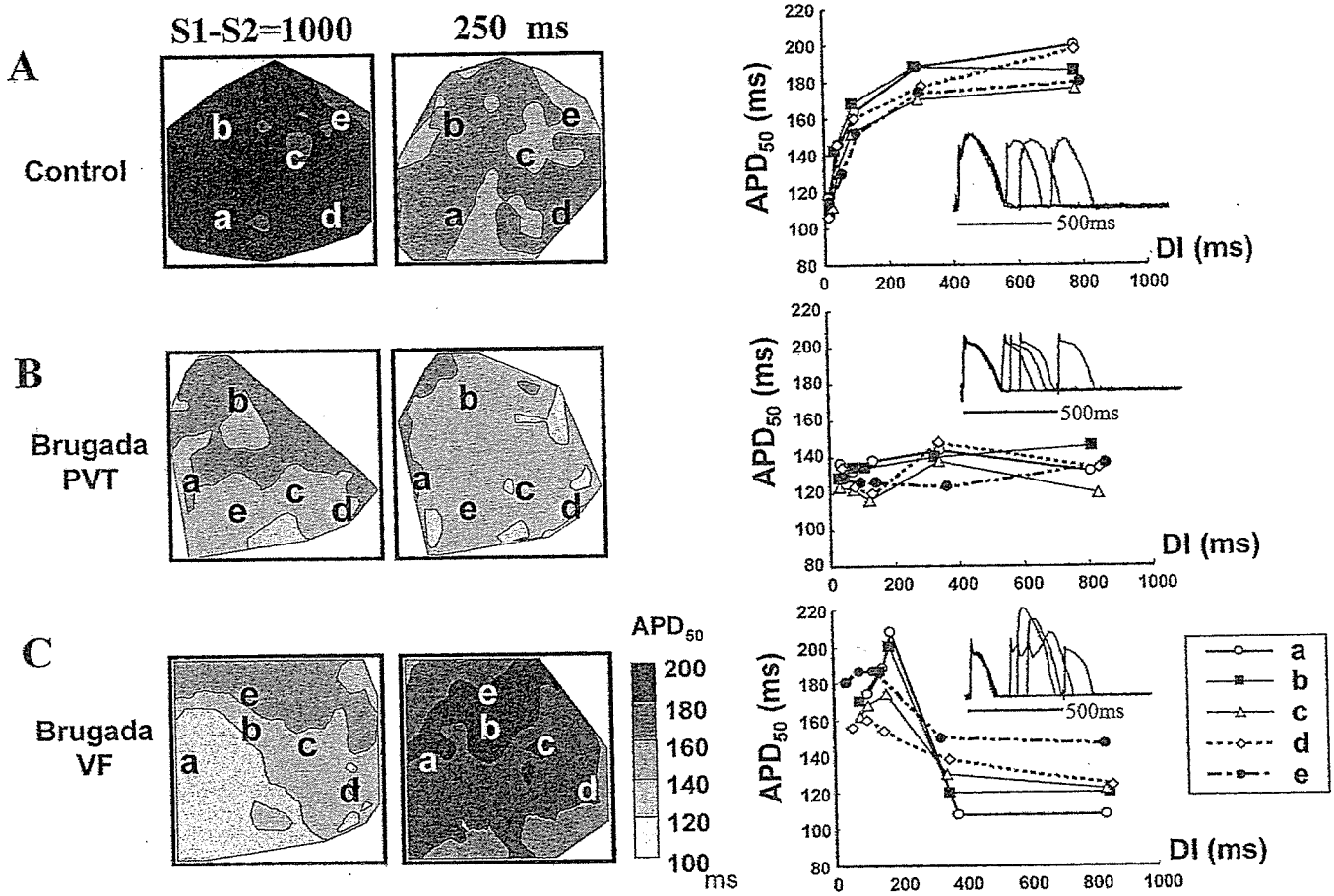

Figure 9. Representative epicardial repolarization maps paced from the epicardium by S1-S2 method and plot of the restitution of action potential duration at each site (**a to e**) and superimposed optical action potentials at site b in control condition (**A**), and the Brugada-ECG condition with polymorphic ventricular tachycardia (PVT) (**B**) or ventricular fibrillation (VF) (**C**). APD_{50} = action potential duration at 50% repolarization; DI = diastolic interval.

ization abnormalities were important in the development of VF. Our results, for the first time, revealed how repolarization and depolarization abnormalities interact in developing a trigger of premature ventricular complexes and in maintaining VF in the Brugada-ECG condition. A steep repolarization gradient in the epicardium introduced P2R-extrasystoles and subsequent non-sustained polymorphic VT, and further increased depolarization and repolarization abnormalities maintained VF, thus increasing risk of sudden cardiac death.

Study limitations. First, we mapped the epicardial or endocardial surface separately in each condition. Therefore, the two-dimensional mapping technique used in this study provides only limited insights into the number of spiral waves and these re-entrant patterns and could not directly evaluate the relationship between the transmural gradient of repolarization and arrhythmogenesis in the Brugada-ECG condition. A second limitation is the size of wedge preparation. It is unclear whether a polymorphic VT or VF in the wedges can result in those with larger hearts. Third, we pharmacologically created, similarly to the methods of previous studies, the Brugada-phenotype, which could not be a complete surrogate for the Brugada syndrome. Finally, with optical mapping, there is a major concern about motion artifacts that can greatly distort the AP recorded, but our ratio-metric methods can reduce motion artifacts without using an uncoupler.

Reprint requests and correspondence: Dr. Wataru Shimizu, Division of Cardiology, Department of Internal Medicine, National Cardiovascular Center, 5-7-1 Fujishiro-dai, Suita, Osaka, 565-8565 Japan. E-mail: wshimizu@hsp.ncvc.go.jp.

REFERENCES

1. Brugada P, Brugada J. Right bundle branch block, persistent ST-segment elevation and sudden cardiac death: a distinct clinical and electrocardiographic syndrome. A multicenter report. J Am Coll Cardiol 1992;20:1391–6.
2. Wilde AA, Antzelevitch C, Borggrefe M, et al. Proposed diagnostic criteria for the Brugada syndrome: consensus report. Circulation 2002; 106:2514–9.
3. Brugada J, Brugada R, Antzelevitch C, Towbin J, Nademanee K, Brugada P. Long-term follow-up of individuals with the electrocardiographic pattern of right bundle-branch block and ST-segment elevation in precordial leads V1 to V3. Circulation 2002;105:73–8.
4. Antzelevitch C, Brugada P, Borggrefe M, et al. Brugada syndrome: report of the second consensus conference: endorsed by the Heart Rhythm Society and the European Heart Rhythm Association. Circulation 2005;111:659–70.
5. Brugada J, Brugada R, Brugada P. Determinants of sudden cardiac death in individuals with the electrocardiographic pattern of Brugada

syndrome and no previous cardiac arrest. Circulation 2003;108: 3092–6.
6. Priori SG, Napolitano C, Gasparini M, et al. Natural history of Brugada syndrome: insights for risk stratification and management. Circulation 2002;105:1342–7.
7. Antzelevitch C, Brugada P, Brugada J, Brugada R, Towbin JA, Nademanee K. Brugada syndrome: 1992–2002: a historical perspective. J Am Coll Cardiol 2003;41:1665–71.
8. Yan GX, Antzelevitch C. Cellular basis for the Brugada syndrome and other mechanisms of arrhythmogenesis associated with ST-segment elevation. Circulation 1999;100:1660–6.
9. Di Diego JM, Cordeiro JM, Goodrow RJ, et al. Ionic and cellular basis for the predominance of the Brugada syndrome phenotype in males. Circulation 2002;106:2004–11.
10. Fish JM, Antzelevitch C. Role of sodium and calcium channel block in unmasking the Brugada syndrome. Heart Rhythm 2004;1:210–7.
11. Kurita T, Shimizu W, Inagaki M, et al. The electrophysiologic mechanism of ST-segment elevation in Brugada syndrome. J Am Coll Cardiol 2002;40:330–4.
12. Lukas A, Antzelevitch C. Phase 2 re-entry as a mechanism of initiation of circus movement re-entry in canine epicardium exposed to simulated ischemia. Cardiovasc Res 1996;32:593–603.
13. Nademanee K, Veerakul G, Nimmannit S, et al. Arrhythmogenic marker for the sudden unexplained death syndrome in Thai men. Circulation 1997;96:2595–600.
14. Kanda M, Shimizu W, Matsuo K, et al. Electrophysiologic characteristics and implications of induced ventricular fibrillation in symptomatic patients with Brugada syndrome. J Am Coll Cardiol 2002;39: 1799–805.
15. Ikeda T, Sakurada H, Sakabe K, et al. Assessment of noninvasive markers in identifying patients at risk in the Brugada syndrome: insight into risk stratification. J Am Coll Cardiol 2001;37:1628–34.
16. Nagase S, Kusano KF, Morita H, et al. Epicardial electrogram of the right ventricular outflow tract in patients with the Brugada syndrome: using the epicardial lead. J Am Coll Cardiol 2002;39:1992–5.
17. Smits JP, Eckardt L, Probst V, et al. Genotype-phenotype relationship in Brugada syndrome: electrocardiographic features differentiate SCN5A-related patients from non-SCN5A-related patients. J Am Coll Cardiol 2002;40:350–6.
18. Akar FG, Spragg DD, Tunin RS, Kass DA, Tomaselli GF. Mechanisms underlying conduction slowing and arrhythmogenesis in nonischemic dilated cardiomyopathy. Circ Res 2004;95:717–25.
19. Kimura M, Kobayashi T, Owada S, et al. Mechanism of ST elevation and ventricular arrhythmias in an experimental Brugada syndrome model. Circulation 2004;109:125–31.
20. Gray RA, Pertsov AM, Jalife J. Spatial and temporal organization during cardiac fibrillation. Nature 1998;392:75–8.
21. Liu YB, Peter A, Lamp ST, Weiss JN, Chen PS, Lin SF. Spatiotemporal correlation between phase singularities and wavebreaks during ventricular fibrillation. J Cardiovasc Electrophysiol 2003;14:1103–9.
22. Pitzalis MV, Anaclerio M, Iacoviello M, et al. QT-interval prolongation in right precordial leads: an additional electrocardiographic hallmark of Brugada syndrome. J Am Coll Cardiol 2003;42:1632–7.
23. Kakishita M, Kurita T, Matsuo K, et al. Mode of onset of ventricular fibrillation in patients with Brugada syndrome detected by implantable cardioverter defibrillator therapy. J Am Coll Cardiol 2000;36: 1646–53.
24. Morita H, Fukushima-Kusano K, Nagase S, et al. Site-specific arrhythmogenesis in patients with Brugada syndrome. J Cardiovasc Electrophysiol 2003;14:373–9.
25. Krishnan SC, Antzelevitch C. Flecainide-induced arrhythmia in canine ventricular epicardium. Phase 2 re-entry? Circulation 1993;87: 562–72.
26. Miyoshi S, Mitamura H, Fujikura K, et al. A mathematical model of phase 2 re-entry: role of L-type Ca current. Am J Physiol Heart Circ Physiol 2003;284:H1285–94.
27. Chen Q, Kirsch GE, Zhang D, et al. Genetic basis and molecular mechanism for idiopathic ventricular fibrillation. Nature 1998;392: 293–6.
28. Brugada R, Brugada J, Antzelevitch C, et al. Sodium channel blockers identify risk for sudden death in patients with ST-segment elevation and right bundle branch block but structurally normal hearts. Circulation 2000;101:510–5.
29. Shimizu W, Antzelevitch C, Suyama K, et al. Effect of sodium channel blockers on ST segment, QRS duration, and corrected QT interval in patients with Brugada syndrome. J Cardiovasc Electrophysiol 2000; 11:1320–9.
30. Gasparini M, Priori SG, Mantica M, et al. Programmed electrical stimulation in Brugada syndrome: how reproducible are the results? J Cardiovasc Electrophysiol 2002;13:880–7.
31. Wu TJ, Lin SF, Weiss JN, Ting CT, Chen PS. Two types of ventricular fibrillation in isolated rabbit hearts: importance of excitability and action potential duration restitution. Circulation 2002;106: 1859–66.
32. Hisamatsu K, Kusano KF, Morita H, et al. Relationships between depolarization abnormality and repolarization abnormality in patients with Brugada syndrome. J Cardiovasc Electrophysiol 2004;15:870–6.
33. Tukkie R, Sogaard P, Vleugels J, de Groot IK, Wilde AA, Tan HL. Delay in right ventricular activation contributes to Brugada syndrome. Circulation 2004;109:1272–7.

APPENDIX

For accompanying videos to Figures 5, 6, and 7, please see the online version of this article.

Am J Physiol Heart Circ Physiol 291: H318–H326, 2006.
First published February 24, 2006; doi:10.1152/ajpheart.00975.2005.

Short-term electroacupuncture at Zusanli resets the arterial baroreflex neural arc toward lower sympathetic nerve activity

Daisaku Michikami,[1,2] Atsunori Kamiya,[1] Toru Kawada,[1] Masashi Inagaki,[1] Toshiaki Shishido,[1] Kenta Yamamoto,[1,2] Hideto Ariumi,[1,2] Satoshi Iwase,[3] Junichi Sugenoya,[3] Kenji Sunagawa,[4] and Masaru Sugimachi[1]

[1]*Department of Cardiovascular Dynamics, Advanced Medical Engineering Center, National Cardiovascular Center Research Institute, Osaka;* [2]*Pharmaceuticals and Medical Devices Agency, Tokyo;* [3]*Department of Physiology, School of Medicine Aichi Medical University, Nagakute, Aichi; and* [4]*Department of Cardiovascular Medicine, Kyushu University Graduate School of Medical Sciences, Fukuoka, Japan*

Submitted 12 September 2005; accepted in final form 17 February 2006

Michikami, Daisaku, Atsunori Kamiya, Toru Kawada, Masashi Inagaki, Toshiaki Shishido, Kenta Yamamoto, Hideto Ariumi, Satoshi Iwase, Junichi Sugenoya, Kenji Sunagawa, and Masaru Sugimachi. Short-term electroacupuncture at Zusanli resets the arterial baroreflex neural arc toward lower sympathetic nerve activity. *Am J Physiol Heart Circ Physiol* 291: H318–H326, 2006. First published February 24, 2006; doi:10.1152/ajpheart.00975.2005.—Although electroacupuncture reduces sympathetic nerve activity (SNA) and arterial pressure (AP), the effects of electroacupuncture on the arterial baroreflex remain to be systematically analyzed. We investigated the effects of electroacupuncture of Zusanli on the arterial baroreflex using an equilibrium diagram comprised of neural and peripheral arcs. In anesthetized, vagotomized, and aortic-denervated rabbits, we isolated carotid sinuses and changed intra-carotid sinus pressure (CSP) from 40 to 160 mmHg in increments of 20 mmHg/min while recording cardiac SNA and AP. Electroacupuncture of Zusanli was applied with a pulse duration of 5 ms and a frequency of 1 Hz. An electric current 10 times the minimal threshold current required for visible muscle twitches was used and was determined to be 4.8 ± 0.3 mA. Electroacupuncture for 8 min decreased SNA and AP (n = 6). It shifted the neural arc (i.e., CSP-SNA relationship) to lower SNA but did not affect the peripheral arc (i.e., SNA-AP relationship) (n = 8). SNA and AP at the closed-loop operating point, determined by the intersection of the neural and peripheral arcs, decreased from 100 ± 4 to 80 ± 9 arbitrary units and from 108 ± 9 to 99 ± 8 mmHg (each $P < 0.005$), respectively. Peroneal denervation eliminated the shift of neural arc by electroacupuncture (n = 6). Decreasing the pulse duration to <2.5 ms eliminated the effects of SNA and AP reduction. In conclusion, short-term electroacupuncture resets the neural arc to lower SNA, which moves the operating point toward lower AP and SNA under baroreflex closed-loop conditions.

arterial pressure; equilibrium diagram

ALTHOUGH THERE ARE MANY clinical case reports (21, 30, 32, 39, 40, 42), the effects of electroacupuncture on cardiovascular regulation remain to be systematically investigated. There has been a recent renewal of interest in the inhibitory effects of electroacupuncture of the Zusanli acupoint on the cardiovascular system, including reductions in arterial pressure (AP), heart rate, (3, 15, 16), and sympathetic nerve activity (SNA) (25, 42). Such inhibitory effects are observed during low-frequency (<20 Hz) electroacupuncture. Because the arterial baroreflex is one of the most important control systems that stabilize AP, we quantified the effects of electroacupuncture on the arterial baroreflex over an entire operating range. Systematic analysis would help to assess the possible utility of electroacupuncture as a treatment modality for certain cardiovascular diseases with vagolytic and sympathotonic states (26, 38).

One of the best ways to quantitatively analyze changes in the arterial baroreflex over an entire operating range may be analysis using a baroreflex equilibrium diagram (10, 23, 31) (see APPENDIX for details). Briefly, the baroreflex equilibrium diagram consists of a neural arc representing SNA as a function of baroreceptor input pressure and a peripheral arc representing AP as a function of SNA. The intersection of the two arcs corresponds to an operating point of the AP regulation under baroreflex closed-loop conditions. Considering the reduced AP and SNA found in previous studies, we hypothesized that short-term electroacupuncture resets the arterial baroreflex neural arc to lower SNA. In the present study, to test this hypothesis, we constructed a baroreflex equilibrium diagram with neural and peripheral arcs in anesthetized rabbits. The present findings indicate that electroacupuncture resets the baroreflex neural arc to lower SNA, moving the closed-loop operating point toward lower AP and SNA.

MATERIALS AND METHODS

Surgical Preparation

Animals were cared for in strict accordance with the *Guiding Principles for the Care and Use of Animals in the Field of Physiological Sciences* approved by the Physiological Society of Japan. Twenty-two Japanese White rabbits weighing 2.4–3.3 kg were anesthetized via intravenous injection (2 ml/kg) with a mixture of urethane (250 mg/ml) and α-chloralose (40 mg/ml) and mechanically ventilated with oxygen-enriched room air. Supplemental doses were injected as necessary (0.5 ml/kg) to maintain an appropriate level of anesthesia. Body temperature was maintained at ~38°C with a heating pad. AP was measured by using a high-fidelity pressure transducer (SPC-330A, Millar Instruments, Houston, TX) inserted via the left femoral artery. To record cardiac SNA, we exposed the left cardiac sympathetic nerve through a midline thoracotomy and attached a pair of stainless steel wire electrodes (Bioflex wire AS633, Cooner Wire, Chatsworth, CA) to the nerve. The nerve fibers peripheral to the

Address for reprint requests and other correspondence: D. Michikami, Dept. of Cardiovascular Dynamics, Advanced Medical Engineering Center, National Cardiovascular Center Research Institute, 5-7-1 Fujishirodai, Suita, Osaka 565–8565, Japan (e-mail: dmichi@ri.ncvc.go.jp or kamiya@ri.ncyc.go.jp).

The costs of publication of this article were defrayed in part by the payment of page charges. The article must therefore be hereby marked "*advertisement*" in accordance with 18 U.S.C. Section 1734 solely to indicate this fact.

electrodes were sectioned to eliminate afferent signals from the heart. To insulate and fix the electrodes, the nerves and electrodes were secured with silicone glue (Kwik-Sil, World Precision Instruments, Sarasota, FL). The preamplified nerve signals were band-pass filtered at 150–1,000 Hz, full-wave rectified, and low-pass filtered at a cutoff frequency of 30 Hz by using analog circuit. After that, the neural signals were recorded at a sampling rate of 200 Hz using a 12-bit analog-to-digital converter. Pancuronium bromide (0.1 mg/kg) was administered to prevent contaminating muscular activities. At the end of the experiment, the experimental animals were killed by an overdose of intravenous pentobarbital sodium, and the background noise level of SNA was determined postmortem.

Sixteen of the 22 rabbits were used in *protocol 1 (protocols 1-1, 1-2, and 1-3)*, and the remaining 6 rabbits were used in *protocols 2, 3,* and *4*. In 10 of the 16 rabbits for *protocols 1-2* and/or *1-3* described below, we isolated both carotid sinuses from the systemic circulation by ligating the internal and external carotid arteries and other small branches originating from the carotid sinus regions. The isolated carotid sinuses were filled with warmed physiological saline through catheters inserted via the common carotid arteries. The intra-carotid sinus pressure (CSP) was controlled by a servo-controlled piston pump (model ET-126A, Labworks, Costa Mesa, CA). In the baroreflex open-loop experimental settings, bilateral vagal and aortic depressor nerves were sectioned at the neck to minimize reflex effects from cardiopulmonary regions and the aortic arch.

Electroacupuncture

Two stainless steel needles were inserted at the one-fifth point (from the knee) and the midpoint of the knee-ankle distance of approximately 30–35 mm. These needles with a diameter of 0.2 mm (CE0123, Seirin-Kasei, Shimizu City, Japan) were inserted to a depth of ~10 mm in the skin and underlying muscle (the right tibialis anterior muscle). This area corresponds to the Zusanli and Xiajuxu acupoints (over the peroneal nerve below the knee, stomach meridian, St 36 and 39) in humans.

As in previous studies (2, 3, 17, 42), the stimulus current intensity was determined as 10 times of twitch threshold, which is the minimal electrical current required for eliciting visible muscle twitches of the stimulated leg. Actually, the current was 4.8 ± 0.3 mA (4.2–5.4 mA). An electric rectangular wave current with a frequency of 1 Hz and with pulse duration of 5 ms was passed between these two needles by using an electrical stimulator (SEN-7203, Nihon Kohden) except *protocol 4* where shorter pulse durations were challenged.

Protocols

The experimental protocol was approved by the Animal Experimental Committee of National Cardiovascular Center Research Institute.

Protocol 1: effect of Zusanli electroacupuncture on AP, SNA, and baroreflex. PROTOCOL 1-1 (BAROREFLEX CLOSED-LOOP CONDITION, N = 6). To elucidate the overall cardiovascular inhibitory effects of electroacupuncture, we performed 1 Hz electroacupuncture for 8 min and measured AP and SNA responses under conditions of intact cardiovascular reflexes. In this closed-loop protocol, vagal and aortic depressor nerves were preserved. Baseline data were measured for 1 min before acupuncture insertion. At 10 min after acupuncture insertion, baseline data were measured again for 1 min. Electroacupuncture was applied for 8 min. The recovery data were measured for 2 min after the cessation of electroacupuncture.

PROTOCOL 1-2 (BAROREFLEX OPEN-LOOP CONDITION, N = 8). To elucidate the effects of electroacupuncture on the arterial baroreflex over an entire operating range, we performed a baroreflex open-loop experiment as follows. CSP was first decreased to 40 mmHg. After attainment of a steady state, CSP was increased from 40 to 160 mmHg in increments of 20 mmHg. Each pressure step was maintained for 60 s. We measured AP and SNA during the stepwise increase in CSP. Two trials (control and electroacupuncture trials) were performed on each rabbit. The order of the trials was randomized. The electroacupuncture trial was identical to the control trial except that electroacupuncture was commenced 1 min before the initiation of stepwise increase in CSP.

PROTOCOL 1-3 (BAROREFLEX OPEN-LOOP CONDITION WITH PERONEAL DENERVATION, N = 6). To identify the afferent pathway of electroacupuncture, we examined the effects of 1 Hz electroacupuncture on the arterial baroreflex after severing the right peroneal nerve at the level of the knee joint. Estimation of the baroreflex equilibrium diagram was conducted as in *protocol 1-2* in the control and electroacupuncture trials. Four of the six rabbits had also undergone *protocol 1-2*.

Protocol 2: effects of sham (nonelectrical) acupuncture at Zusanli and control (nonspecific) electrical and nonelectrical acupunctures on AP and SNA in baroreflex closed-loop condition (n = 6). To determine whether changes in AP and SNA during Zusanli electroacupuncture are specific responses, sham and control acupunctures were conducted under the following acupuncture conditions: *1*) no acupuncture (nonacupuncture), *2*) nonelectrical acupuncture at Zusanli-Xiajuxu (St 36–39) acupoints (sham acupuncture), *3*) nonelectrical acupuncture at Guangming-Xuanzhong (gallbladder meridian, Gb 37–39) acupoints (control acupuncture), and *4*) electrical acupuncture at Guangming-Xuanzhong acupoints (control electroacupuncture). We chose Guangming-Xuanzhong as nonspecific control acupoints (*trials 3* and *4*) because these acupoints are believed to reduce leg pain without affecting the cardiovascular system, in contrast to the Zusanli-Xiajuxu acupoints. In each trial, AP and SNA were measured for a baseline duration of 1 min, under acupuncture condition (*trial 1, 2, 3,* or *4*) for 8 min, and recovery for 1 min.

Protocol 3: effect of long-term Zusanli electroacupuncture on AP and SNA in baroreflex closed-loop condition (n = 6). To clarify the effect of long-term electroacupuncture on cardiovascular system, AP and SNA were measured during and after 30 min of electroacupuncture at Zusanli-Xiajuxu acupoints. *Protocol 3* was conducted in the same manner as *protocol 1-1* except with a longer stimulation duration than *protocol 1-1* (8 min).

Protocol 4: Effect of pulse duration of Zusanli electroacupuncture on AP and SNA in baroreflex closed-loop condition (n = 6). To examine the effect of pulse duration of electroacupuncture on AP and SNA, AP and SNA were measured during electroacupuncture at Zusanli-Xiajuxu acupoints with the pulse duration increasing stepwise from 0.1 to 0.25, 0.5, 1, 2.5, 5, and 10 ms, every 60 s. In each animal, the frequency and stimulus current intensity were maintained constant as in *protocols 1, 2,* and *3*.

Data Analysis

We recorded CSP, SNA, and AP at a sampling rate of 200 Hz by using a 12-bit analog-to-digital converter. Data were stored on the hard drive of a dedicated laboratory computer system for later analyses.

In *protocol 1-1, 2, and 4*, mean AP and SNA for 1 min were calculated for baseline conditions, every minute of electroacupuncture, and recovery. In *protocol 3*, mean AP and SNA for 5 min were calculated for baseline conditions, electroacupuncture, and recovery. In *protocols 1-2* and *1-3*, we calculated mean AP and SNA during the last 10 s of each CSP step. Because the absolute magnitude of SNA depended on recording conditions, SNA was presented in arbitrary units (au). The background noise level was set at 0 au and the SNA value at the closed-loop operating point in the control trial (without electroacupuncture) was set at 100 au for each animal.

A four-parameter logistic function analysis was performed on the neural arc (CSP-SNA data pairs) and the peripheral arc (SNA-AP data pairs) as follows (11)

$$y = \frac{P_1}{1 + \exp[P_2(x - P_3)]} + P_4 \quad (1)$$

where x and y represent the input and the output, respectively. P_1 denotes the response range (i.e., the difference between the maximum and minimum values of y), P_2 is the coefficient of gain, P_3 is the midpoint of the logistic function on the input axis, and P_4 is the minimum value of y. The maximum gain (G_{max}) is calculated from $-P_1P_2/4$ at $x = P_3$. The parameter values were calculated by an iterative nonlinear least-squares regression known as the downhill simplex method.

Statistical Analysis

All data are presented as means ± SD. Differences were considered to be significant when $P < 0.05$. In *protocols 1-1, 2, 3,* and *4*, the effects of electroacupuncture on AP and SNA at different time intervals were evaluated by one-way ANOVA. The Dunnett's test was used for multiple comparisons. In *protocols 1-2* and *1-3*, the effects of electroacupuncture on the four parameters of the logistic functions relating to the neural and peripheral arcs, as well as on the closed-loop operating point, were examined by using a paired *t*-test.

RESULTS

Figure 1*A* (*protocol 1-1*) shows a typical time series of AP and SNA in response to Zusanli-Xiajuxu electroacupuncture with intact cardiovascular reflexes. AP and SNA were reduced immediately after beginning electroacupuncture, and these remained reduced during 8-min electroacupuncture. Figure 1*B* illustrates the group-averaged AP and SNA in response to electroacupuncture. AP and SNA for baseline were unchanged by acupuncture insertion alone, while these values for 8-min electroacupuncture remained decreased from baseline. These values returned to baseline level after the cessation of electroacupuncture.

Figure 2 (*protocol 1-2*) shows a typical AP and SNA response to the increments in CSP in the control (Fig. 2, *left*) and electroacupuncture (Fig. 2, *right*) trials. A stepwise increase in CSP decreased SNA and AP in both trials. In the electroacupuncture trial, the AP and SNA response ranges to CSP were attenuated compared with the control trial.

Figure 3, *A* and *B* (*protocol 1-2*), shows the averaged baroreflex neural and peripheral arcs obtained in control and electroacupuncture trials. The neural arc showed a sigmoidal relationship between CSP and SNA. In the neural arc, the response range of SNA (P_1) and midpoint of the operating range (P_3) were significantly decreased by electroacupuncture (Table 1). The coefficient of gain (P_2), the minimum value of SNA (P_4), and G_{max} did not differ between the two trials (Table 1). As a result, the maximum value of SNA, calculated from $P_1 + P_4$, was significantly decreased by electroacupuncture from 162 ± 31 to 130 ± 29 au ($P < 0.005$). The peripheral arc showed a more linear relationship between SNA and AP than the neural arc. In the peripheral arc, electroacupuncture did not affect any of the four parameters or G_{max} (Table 1 and Fig. 3*B*). The operating point determined by the intersection of the neural and peripheral arcs was moved toward lower AP and SNA (from *point a* to *point b*) by electroacupuncture (Fig. 3*C* and Table 1).

Figure 4 (*protocol 1-3*) shows the averaged baroreflex neural (Fig. 4*A*) and peripheral arcs (Fig. 4*B*) in control and electroacupuncture trials with severance of the peroneal nerve innervating the tibialis anterior muscle. Two arcs obtained in both trials were nearly superimposable. The four parameters and G_{max} in the neural and peripheral arcs and operating point were

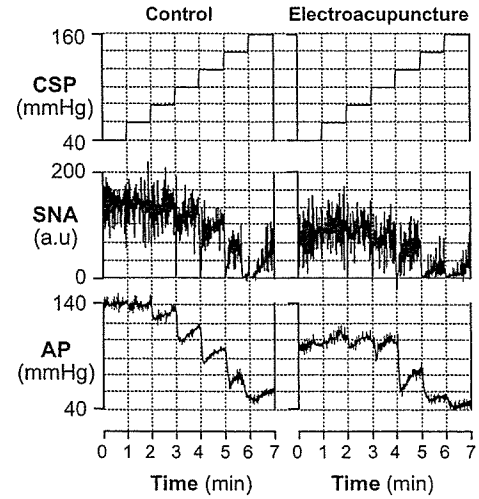

Fig. 2. Typical time series of intra-carotid sinus pressure (CSP), AP, and SNA in control (*left*) and electroacupuncture trials (*right*) in *protocol 1-2*. SNA and AP decreased in response to increments in CSP in both of the two trials. The response ranges of AP and SNA to CSP were lower in electroacupuncture than in controls.

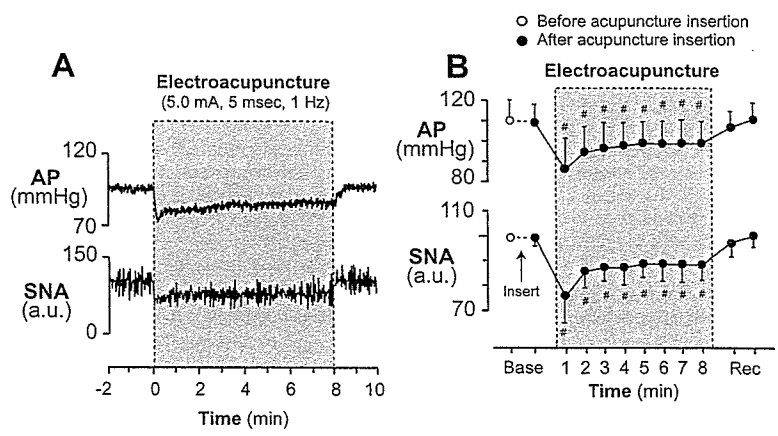

Fig. 1. Typical time series of arterial pressure (AP) and sympathetic nerve activity (SNA) during 8 min of 1-Hz electroacupuncture (*A*) and the averaged ($n = 6$) AP and SNA (*B*) in *protocol 1-1*. Data include periods of baseline (Base, 1 min), electroacupuncture (8 min), and recovery (Rec, 1 min). Each data point represents average values over 1 min. #$P < 0.05$: significantly different from baseline after acupuncture insertion. au, Arbitrary units.

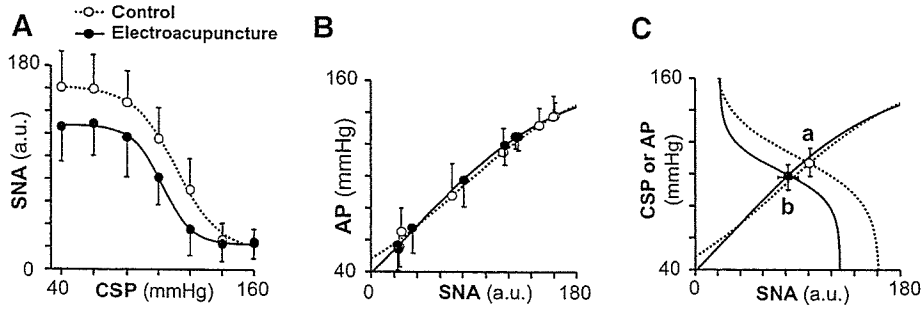

Fig. 3. Averaged (n = 8) baroreflex neural arc (*A*), peripheral arc (*B*), and baroreflex equilibrium diagram (*C*) obtained in 8 rabbits in control (○) and electroacupuncture (●) trials in *protocol 1-2*. Electroacupuncture shifted the neural arc to lower SNA (*A*), but it did not change the peripheral arc (*B*). The shift in neural arc reduced AP and SNA by 9 ± 3 mmHg and 20 ± 10 au (from *point a* to *point b*) at the operating point (*C*).

not affected by electroacupuncture when the peroneal nerve was denervated (Table 2 and Fig. 4*C*).

Figure 5 (*protocol 2*) shows the changes in AP and SNA during nonacupuncture (without acupuncture), sham acupuncture [nonelectrical acupuncture at Zusanli-Xiajuxu (St 36–39)], control acupuncture [nonelectrical acupuncture at Guangming-Xuanzhong (Gb 37–39)] and control electroacupuncture (electrical acupuncture at Gb 37–39) trials. AP and SNA did not change in these trials.

Figure 6, *A* and *B* (*protocol 3*), shows a typical time series and the averaged data, respectively, of AP and SNA in response to long-term Zusanli-Xiajuxu electroacupuncture. AP and SNA decreased immediately after electroacupuncture was started and remained reduced during 30-min electroacupuncture. In addition, AP and SNA returned to the preelectroacupuncture baseline levels immediately after cessation of electroacupuncture.

Figure 7, *A* and *B* (*protocol 4*), shows a typical time series and the averaged data, respectively, of AP and SNA during Zusanli-Xiajuxu electroacupuncture with the pulse duration increasing from 0.1 to 5 ms. Although increasing the pulse duration from 0.1 to 1 ms did not change AP and SNA, pulse durations of 2.5 ms and higher decreased SNA while pulse durations of 5 and 10 ms decreased AP.

Table 1. *Effect of electroacupuncture on the operating point of baroreflex and on the 4 parameters of logistic functions approximating neural and peripheral baroreflex arcs*

	Control	Electroacupuncture
Operating point		
Arterial pressure, mmHg	108.4±8.7	98.8±7.9†
Sympathetic nerve activity, au	99.8±4.1	80.0±8.9†
Neural arc		
P_1, au	144.0±35.0	112.6±9.2†
P_2, au/mmHg	0.08±0.03	0.09±0.09
P_3, mmHg	111.4±6.5	103.3±10.0*
P_4, au	17.5±6.1	17.4±8.7
G_{max}, au/mmHg	−2.94±0.91	−2.58±1.27
Peripheral arc		
P_1, mmHg	129.6±20.5	125.9±19.5
P_2, au/mmHg	−0.03±0.01	−0.03±0.01
P_3, au	80.6±23.2	71.7±17.1
P_4, mmHg	29.9±16.3	29.5±12.1
G_{max}, mmHg/au	0.74±0.10	0.84±0.18

Values are means ± SD (n = 8). G_{max}, maximum gain. See *Data Analysis* for definition of 4 parameters of logistic function. au, Arbitrary units. *P < 0.05 and †P < 0.005 vs. control.

DISCUSSION

The major new finding of the present study was that electroacupuncture at Zusanli resets the arterial baroreflex neural arc to lower SNA but does not significantly affect the baroreflex peripheral arc. As a result, the operating point determined by the intersection of the neural and peripheral arcs was moved toward lower SNA and AP by electroacupuncture. To the best of our knowledge, this is the first study delineating the effects of short-term electroacupuncture on the arterial baroreflex over an entire operating range.

Effects of Electroacupuncture on the Arterial Baroreflex (Protocol 1)

The arterial baroreflex system is one of the most important negative-feedback systems that stabilize AP against exogenous disturbances. When AP is decreased by exogenous perturbation such as blood loss, the reduction in AP is sensed by the arterial baroreceptors. SNA is then increased by the arterial baroreflex to buffer the reduction in AP. In such circumstances, SNA and AP change reciprocally. On the other hand, when SNA is changed by an exogenous perturbation such as emotional stress, SNA and AP change in parallel. In *protocol 1-1*, electroacupuncture decreased both SNA and AP, indicating that electroacupuncture introduced exogenous perturbation to decrease SNA with a resultant reduction in AP. Although the net effect of electroacupuncture is to decrease SNA, the perturbation of AP cannot be excluded. For example, because electroacupuncture also twitched the hindlimb muscles, electroacupuncture might have perturbed AP via changes in vascular resistance and/or venous return through muscle pump function. Therefore, to quantify the contribution of both perturbations on SNA and on AP, we performed *protocol 1-2*. Perturbation of AP is most easily detected by comparing AP at the same SNA level with and without electroacupuncture.

In *protocol 1-2*, we performed a baroreflex open-loop experiment and identified the static characteristics of the neural and peripheral arcs over a wide operating range. As expected, electroacupuncture shifted the neural arc toward lower SNA and decreased maximum SNA to ~80% of control (Fig. 3*A*). This shift is not due to reduced perfusion to the medulla by AP reduction during electroacupuncture because the AP was decreased by ~10 mmHg and would not induce cerebral ischemia. In contrast, electroacupuncture had little effect on the peripheral arc (Fig. 3*B*). In other words, AP with and without electroacupuncture did not differ significantly at any of the SNA levels. Therefore, changes in AP observed in *protocol 1-1*

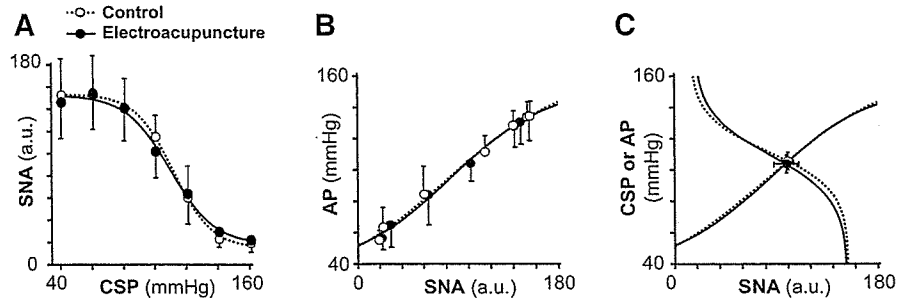

Fig. 4. Averaged (n = 6) baroreflex neural arc (*A*), peripheral arc (*B*), and baroreflex equilibrium diagrams (*C*) obtained in 6 rabbits in control (○) and electroacupuncture (●) trials with peroneal denervation in *protocol 1-3*. The baroreflex neural arc, peripheral arc, and the operating point were not influenced by electroacupuncture after peroneal denervation.

were attributable exclusively to perturbation of SNA and not to possible perturbation effects of electroacupuncture on AP.

The neural and peripheral arcs were combined to yield a baroreflex equilibrium diagram (Fig. 3*C*). The closed-loop operating point, determined by the intersection of the neural and peripheral arcs, moved from *point a* to *point b* during electroacupuncture. Despite a significant shift in the closed-loop operating point, neither the neural nor peripheral arc gain was altered significantly (Table 1). The fact that the baroreflex gain was maintained during electroacupuncture suggests the possible application of electroacupuncture to the treatment of cardiovascular diseases with sympathetic hyperactivity. However, the preservation of the arterial baroreflex gain in the present experimental settings may rely on normal peripheral arc characteristics. Cardiovascular diseases such as heart failure may decrease the peripheral arc gain to a variable extent due to impaired pump function. Whether the arterial baroreflex function during electroacupuncture can be maintained in cardiovascular diseases awaits future study.

Mechanisms for the Cardiovascular Inhibitory Effects of Electroacupuncture (Protocol 1)

The resetting in the baroreflex neural arc during electroacupuncture was mediated by a somatosympathetic reflex arising from the stimulated hindlimb, as evidenced by the fact that peroneal denervation abolished the resetting (Table 2 and Fig. 4). This result was consistent with an earlier study (27) showing that depressor and sympathoinhibitory responses during acupuncture were abolished by sciatic and femoral denervation. The existence of a somatosympathetic reflex is also supported by the fact that electrical stimulation of somatic afferents reduced AP (7–9). Legramante et al. (14) showed that rapidly conducting group III somatic afferent activation can evoke AP reduction during 1-Hz electrical stimulation of the tibial nerve. In contrast, high-frequency stimulation of the somatic afferent evokes AP elevation. Passive muscle stretching, which is considered to activate group III somatic afferent fibers, shifts the baroreflex neural arc toward higher SNA, resulting in an increase in the closed-loop operating point (41). The mechanism of two opposing influences of somatic afferent activation depending on the stimulation frequency is not fully understood.

Table 2. *Effect of electroacupuncture with peroneal denervation on the operating point of baroreflex and on the 4 parameters of logistic functions approximating neural and peripheral baroreflex arcs*

	Control	Electroacupuncture
Operating point		
Arterial pressure, mmHg	105.7±5.7	104.1±5.6
Sympathetic nerve activity, au	99.8±5.1	98.3±11.1
Neural arc		
P_1, au	138.3±42.4	136.3±38.6
P_2, au/mmHg	0.11±0.03	0.08±0.03
P_3, mmHg	112.7±10.2	111.5±10.6
P_4, au	14.9±8.7	15.7±7.4
G_{max}, au/mmHg	−3.27±1.15	−2.84±1.12
Peripheral arc		
P_1, mmHg	144.1±35.5	140.5±34.4
P_2, au/mmHg	−0.02±0.002	−0.02±0.004
P_3, au	82.0±34.0	78.8±32.0
P_4, mmHg	26.1±8.1	25.5±5.3
G_{max}, mmHg/au	0.69±0.13	0.72±0.21

Values are means ± SD (n = 6). See *Data Analysis* for definition of 4 parameters of logistic function.

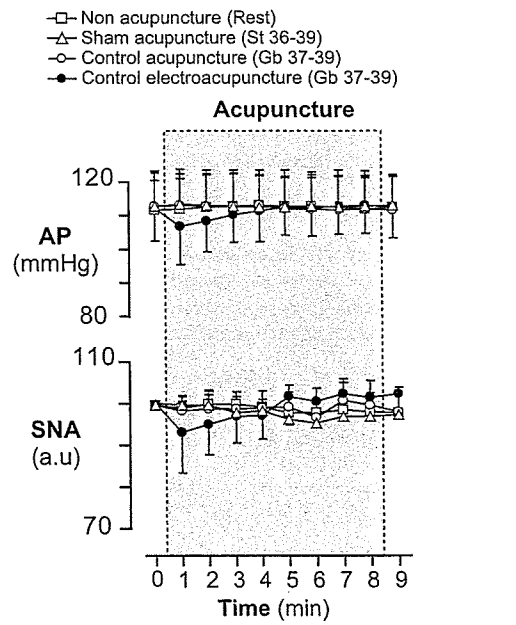

Fig. 5. Averaged (n = 6) AP (*top*) and SNA (*bottom*) in nonacupuncture (condition without acupuncture, □), sham acupuncture [nonelectrical acupuncture at Zusanli-Xiajuxu (stomach meridian, St 36–39), △], control acupuncture [nonelectrical and acupuncture at Guangming-Xuanzhong (gallbladder meridien, Gb 37–39), ○], and control electroacupuncture [electrical acupuncture at Gb 37–39, ●] trials in *protocol 2*. Data include periods of baseline (1 min), electroacupuncture (8 min), and recovery (1 min). Each data point represents average values over 1 min.

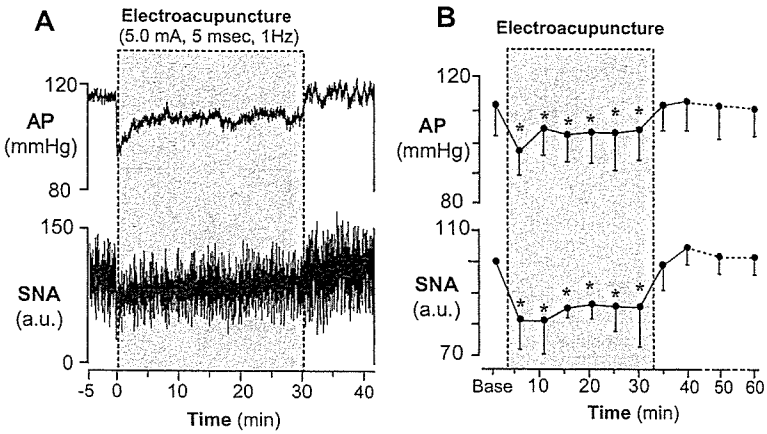

Fig. 6. Typical time series of AP and SNA during 30 min of 1-Hz electroacupuncture (St 36–39; *A*) and the averaged (n = 6) AP and SNA (*B*) in *protocol 3*. Data include periods of baseline (5 min), electroacupuncture (30 min), and recovery (30 min). Each data point represents averaged values over 5 min during baseline, electroacupuncture, and the first 10 min of recovery and those over 10 min during the last 20 min of recovery. *$P < 0.05$: significantly different from baseline after acupuncture insertion.

Another explanation for resetting in the neural arc may be circulatory endogenous opioids (e.g., β-endorphin and enkephalin), which are released from the adrenal gland and hypothalamus by prolonged (>30 min) electroacupuncture (20, 21). These endogenous opioids are known to modulate the arterial baroreflex (24, 29, 35). However, changes in endogenous opioids are unlikely to be the mechanism for reductions in SNA and AP by electroacupuncture in the present experimental settings because the inhibitory effects terminated immediately after cessation of electroacupuncture rather than lasting for several hours (42) (Fig. 1).

Previous studies suggest a central interaction between an electroacupuncture-evoked somatosympathetic reflex and the arterial baroreflex. Baroreceptor afferent inputs inhibit neural activities in the rostral ventrolateral medulla (rVLM) (6, 33). Tjen-A-Looi et al. (36) showed that electroacupuncture inhibited rVLM neural activities, suggesting that the electroacupuncture-evoked somatosympathetic reflex and arterial baroreflex share common central pathways. In addition, 2-Hz electroacupuncture inhibits SNA through the excitation of β-endorphinergic and GABAergic neurons to rVLM (12, 13).

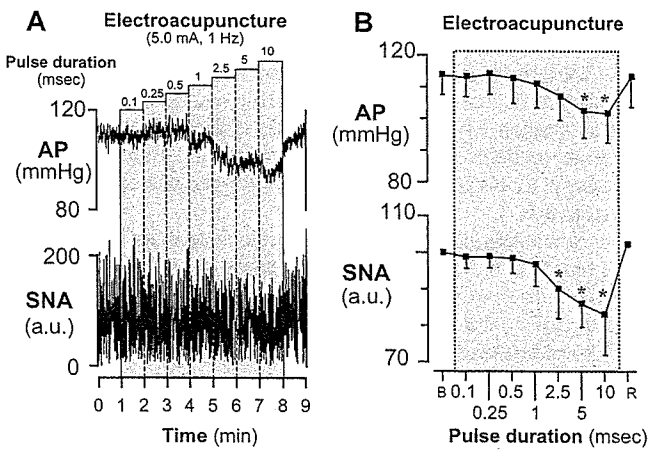

Fig. 7. Typical time series of AP and SNA during 1-Hz electroacupuncture with increasing the pulse duration (*A*) and the averaged (n = 6) AP and SNA (*B*) in *protocol 4*. Data include periods of baseline (B, 1 min), electroacupuncture (7 min), and recovery (R, 1 min). Each data point represents average values over 1 min. *$P < 0.05$; significantly different from baseline after acupuncture insertion.

Central interaction in the brain stem may be involved in the resetting of the arterial baroreflex neural arc induced by electroacupuncture.

Characteristics of Zusanli-Xiajuxu Electroacupuncture Used in the Present Study

The Zusanli electroacupuncture used in this study has some unique characteristics. First, our results showed that baseline AP and SNA were decreased significantly by electroacupuncture, in contrast to previous studies that found no significant reduction in baseline AP and SNA during Zusanli electroacupuncture in rats (0.5-ms duration, 1–2 mA, 2 Hz) (18) and nonelectrical acupuncture in normotensive humans (right large intestine 4, right liver 3, and left spleen 6) (22). Second, our result showed that AP and SNA were reduced as soon as electroacupuncture was started, in contrast to previous reports that the effect of Zusanli electroacupuncture did not even begin to manifest for the first 10–15 min in rats (0.5-ms duration, 1–2 mA, 2 Hz) (18) and cats (0.5-ms duration, 0.4–0.6 mA, 2–4 Hz) (37). These discrepancies may be related to the differences in acupoints and stimulation conditions (pulse duration, current, and frequency). In particular, the pulse duration used in our study (5 ms) was approximately 10–50 times longer than that used in previous studies. Indeed, the data obtained from *protocol 4* show that increasing the pulse duration augments the reduction in AP and SNA during electroacupuncture; pulse durations shorter than 2.5 ms did not change AP and SNA, whereas durations of 2.5 ms and above decreased both parameters immediately after the electroacupuncture was started (Fig. 7). In addition, our data suggest that stimulation duration (<2.5 ms) does not affect arterial baroreflex, consistent with our preliminary data that baroreflex neural, peripheral, and total arcs remained unchanged during electroacupuncture with pulse durations <2.5 ms (unpublished data). These observations may indicate that the effect of electroacupuncture on arterial baroreflex is linked to the stimulation pulse duration.

The third characteristic is that the inhibitory effects of electroacupuncture on AP and SNA disappeared immediately after the cessation of electroacupuncture. In contrast, some studies showed that the inhibitory effects of electroacupuncture on AP lasted for 10–60 min after the cessation (18). The characteristics in this study may not be explained by the length of electroacupuncture because AP and SNA recovered to the

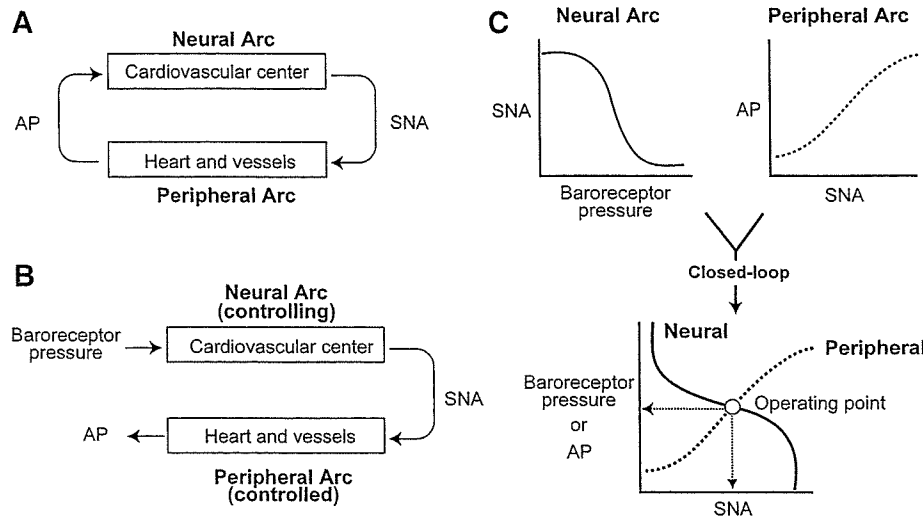

Fig. 8. Arterial baroreflex system in closed-loop (*A*) and open-loop (*B*) conditions. In open-loop conditions, the relationships between baroreceptor pressure and SNA (the neural arc) and between SNA and AP (the peripheral arc) can be quantitatively measured. Intersection of the neural and peripheral arcs corresponds to the operating point of AP and SNA under closed-loop conditions of feedback (*C*).

prestimulation baseline levels immediately after the cessation in both short-duration (8 min, Fig. 1) and longer-duration electroacupuncture (30 min, Fig. 6) protocols. The rapid disappearance of effects suggests that the AP and SNA reductions seen in the present study may not be elicited by the opioid mechanism, although clinical experiments with longer-duration electroacupuncture have demonstrated long-lasting effects on the cardiovascular system, which are attributed to opioid substances (2, 12, 15, 37, 42).

The reductions in AP and SNA during Zusanli electroacupuncture seen in the present study may not be just a nonspecific response to acupunctures. Our data from *protocol 2* (Fig. 5) showed that nonelectrical acupuncture at Zusanli (sham acupuncture) did not decrease AP and SNA, suggesting that the AP and SNA reductions during Zusanli electroacupuncture are not simply the results from insertion of acupuncture needles. Furthermore, acupuncture at Guangming-Xuanzhong (control acupuncture, control electroacupuncture) did not change AP and SNA regardless of electrical stimulation (Fig. 5). This result suggests the importance of acupoint specificity and is consistent with an earlier study showing point-specific differences in cardiovascular inhibitory responses (Jiangshi-Neiguan or Shousanli-Quchi acupoints vs. Pianli-Wenlui or Zusanli-Shangjuxu acupoints) (37). These observations may support the concept that Zusanli acupuncture changes cardiovascular variables in experimental animal models (4, 25, 28) and confers beneficial effects on cardiovascular diseases (5, 30, 34), whereas Guangming-Xuanzhong acupuncture does not affect cardiovascular variables (18).

Limitations

There are several limitations to this study. First, as anesthesia affects the autonomic nervous system, the results might have been different without anesthesia. Second, our isolation of the carotid sinus regions may stimulate carotid chemoreceptors. However, in determining baroreflex function, this factor was present in trials with and without electroacupuncture. Therefore, we believe that this factor may not affect our conclusion of baroreflex resetting during electroacupuncture.

Third, acupuncture was inserted at a point corresponding to the Zusanli acupoint in humans. When acupuncture is properly inserted at the acupoint, the patient feels heaviness or soreness. Such sensory information is not available in an anesthetized animal. Because electroacupuncture (as distinct from acupuncture with no electrical stimulation) stimulates not only the inserted point but also the surrounding area, it has been used as a convenient way of stimulating acupoints in patients and in experimental animals. Thus, even if we failed to insert the needle at the precise acupoint, we believe that Zusanli could be stimulated electrically.

Fourth, although we determined the effects of electroacupuncture at Zusanli acupoints on cardiovascular and baroreflex systems, there are other important acupoints that are able to influence these systems. In particular, Neiguan electroacupuncture is actually known to decrease sympathetic premotor neuron activity for a longer period than Zusanli electroacupuncture (36, 37). Further studies are necessary to determine the effect of Neiguan electroacupuncture on the arterial baroreflex.

Last, we evaluated the effects of Zusanli electroacupuncture on the baroreflex function for a short acupuncture duration of only 8 min. Because electroacupuncture is typically practiced for longer periods of time, our results have limited applicability. However, the electroacupuncture we used decreased AP and SNA immediately after application, showing that the procedure has acute effect on the cardiovascular system. That was the reason why we focused on the effect of short duration electroacupuncture on the baroreflex system. Future study is necessary to examine the effects of longer-duration electroacupuncture.

In conclusion, 1 Hz, short-term electroacupuncture of Zusanli reset the baroreflex neural arc toward lower SNA but did not affect the peripheral arc. The closed-loop operating point determined by the intersection of the neural and peripheral arcs was moved toward lower SNA and AP by electroacupuncture.

APPENDIX

Theoretical Considerations: Coupling of Neural and Peripheral Arcs

Changes in AP are immediately sensed by arterial baroreceptors, which alter efferent SNA via the cardiovascular center of baroreflex (Fig. 8*A*). Efferent SNA in turn governs heart rate and the mechanical

properties of the heart and vessels, which themselves exert a direct influence over AP. This negative-feedback loop makes it difficult to analyze the behavior of the arterial baroreflex. To overcome this problem, we opened the negative-feedback loop and divided the system into controlling and controlled elements (31). We defined the controlling element as the neural arc and the controlled element as the peripheral arc (Fig. 8*B*). In the neural arc, the input is the pressure sensed by the arterial baroreceptors and the output is SNA. In the peripheral arc, the input is SNA and the output is AP (Fig. 8*C*). Because pressure sensed by the arterial baroreceptor is equilibrated with AP under physiological conditions, we superimposed the functions of the two arcs and determined the operating point of the system from the intersection of the two arcs. The operating point is defined as the AP and SNA under closed-loop conditions of the feedback system. The validity of this framework has been examined in previous studies (10, 31). Using the baroreflex equilibrium diagram, we aimed to quantify the effects of electroacupuncture on the arterial baroreflex.

GRANTS

This study was supported by Health and Labor Sciences Research Grant for Research on Advanced Medical Technology from the Ministry of Health, Labour, and Welfare of Japan (H14-Nano-002), by a Grant-in-Aid for Scientific Research (A) (15200040) from the Japan Society for the Promotion of Science, the Program for Promotion of Fundamental Studies in Health Science from the Pharmaceutical and Medical Devices Agency of Japan, and by the "Ground-based Research Announcement for Space Utilization" project promoted by Japan Space Forum. This study was also supported by Industrial Technology Research Grant Program in 03A47075 from New Energy and Industrial Technology Development Organization (NEDO) of Japan.

REFERENCES

1. **Brickman AL, Calaresu FR, and Mogenson GJ.** Bradycardia during stimulation of the septum and somatic afferents in the rabbit. *Am J Physiol Regul Integr Comp Physiol* 236: R225–R230, 1979.
2. **Chao DM, Shen LL, Tjen-A-Looi S, Pitsillides KF, Li P, and Longhurst JC.** Naloxone reverses inhibitory effect of electroacupuncture on sympathetic cardiovascular reflex responses. *Am J Physiol Heart Circ Physiol* 276: H2127–H2134, 1999.
3. **Chen S and Ma SX.** Nitric oxide in the gracile nucleus mediates depressor response to acupuncture (ST36). *J Neurophysiol* 90: 780–785, 2003.
4. **Chiu DTJ and Cheng KK.** A study of the mechanism of the hypotensive effect of acupuncture in the rat. *Am J Chin Med* 2: 413–419, 1974.
5. **Chiu YJ, Chi A, and Reid IA.** Cardiovascular and endocrine effects of acupuncture in hypertensive patients. *Clin Exp Hypertens* 19: 1047–1063, 1997.
6. **Dampney RA, Horiuchi J, Tagawa T, Fontes MA, Potts PD, and Polson JW.** Medullary and supramedullary mechanisms regulating sympathetic vasomotor tone. *Acta Physiol Scand* 177: 209–218, 2003.
7. **Johansson B.** Studies on cardiovascular responses induced by electrical stimulation of afferent somatic nerves. A preliminary report. *Med Exp Int J Exp Med* 5: 447–453, 1961.
8. **Johansson B.** Circulatory responses to stimulation of somatic afferents with special reference to depressor effects from muscle nerves. *Acta Physiol Scand Suppl* 198: 1–91, 1962.
9. **Johansson B, Lundgren O, and Mellander S.** Reflex influence of "somatic pressor and depressor afferents" on resistance and capacitance vessels and on transcapillary fluid exchange. *Acta Physiol Scand* 62: 280–286, 1964.
10. **Kawada T, Shishido T, Inagaki M, Zheng C, Yanagiya Y, Uemura K, Sugimachi M, and Sunagawa K.** Estimation of baroreflex gain using a baroreflex equilibrium diagram. *Jpn J Physiol* 52: 21–29, 2002.
11. **Kent BB, Drane JW, Blumenstein B, and Manning JW.** A mathematical model to assess changes in the baroreceptor reflex. *Cardiology* 57: 295–310, 1972.
12. **Ku YH and Chang YZ.** β-Endorphin- and GABA-mediated depressor effect of specific electroacupuncture surpasses pressor response of emotional circuit. *Peptides* 22: 1465–1470, 2001.
13. **Ku YH and Zou CJ.** Beta-endorphinergic neurons in nucleus arcuatus and nucleus tractus solitarii mediated depressor-bradycardia effect of "Tinggong" 2-Hz electroacupuncture. *Acupunct Electrother Res* 18: 175–184, 1993.
14. **Legramante JM, Raimondi G, Adreani CM, Sacco S, Iellamo F, Peruzzi G, and Kaufman MP.** Group III muscle afferents evoke reflex depressor responses to repetitive muscle contractions in rabbits. *Am J Physiol Heart Circ Physiol* 278: H871–H877, 2000.
15. **Li L, Yin-Xiang C, Hong X, Peng L, and Da-Nian Z.** Nitric oxide in vPAG mediates the depressor response to acupuncture in stress-induced hypertensive rats. *Acupunct Electrother Res* 26: 165–170, 2001.
16. **Li P.** The effect of acupuncture on blood pressure: the interrelation of sympathetic activity and endogenous opeoid peptides. *Acupunct Electrother Res* 8: 45–56, 1983.
17. **Li P, Pitsillides KF, Rendig SV, Pan HL, and Longhurst JC.** Reversal of reflex-induced myocardial ischemia by median nerve stimulation: a feline model of electroacupuncture. *Circulation* 97: 1186–1194, 1998.
18. **Li P, Rowshan K, Crisostomo M, Tjen-A-Looi SC, and Longhurst JC.** Effect of electroacupuncture on pressor reflex during gastric distension. *Am J Physiol Regul Integr Comp Physiol* 283: R1335–R1345, 2002.
19. **Li P, Tjen-A-Looi S, and Longhurst JC.** Rostral ventrolateral medullary opioid receptor subtypes in the inhibitory effect of electroacupuncture on reflex autonomic response in cats. *Auton Neurosci* 89: 38–47, 2001.
20. **Lin JG, Chang SL, and Cheng JT.** Release of beta-endorphin from adrenal gland to lower plasma glucose by the electroacupuncture at Zhongwan acupoint in rats. *Neurosci Lett* 326: 17–20, 2002.
21. **Lin JG, Lo MW, Wen YR, Hsieh CL, Tsai SK, and Sun WZ.** The effect of high and low frequency electroacupuncture in pain after lower abdominal surgery. *Pain* 99: 509–514, 2002.
22. **Middlekauff HR, Yu JL, and Hui K.** Acupuncture effects on reflex responses to mental stress in humans. *Am J Physiol Regul Integr Comp Physiol* 280: R1462–R1468, 2001.
23. **Mohrman DE and Heller LJ.** *Cardiovascular Physiology* (4th ed.). New York: McGraw-Hill, 1997, p. 158–230.
24. **Moore PG, Quail AW, Cottee DB, McIlveen SA, and White SW.** Effect of fentanyl on baroreflex control of circumflex coronary conductance. *Clin Exp Pharmacol Physiol* 27: 1028–1033, 2000.
25. **Mori H, Uchida S, Ohsawa H, Noguchi E, Kimura T, and Nishijo K.** Electro-acupuncture stimulation to a hindpaw and a hind leg produces different reflex responses in sympathoadrenal medullary function in anesthetized rats. *J Auton Nerv Syst* 79: 93–98, 2000.
26. **Nishijo K, Mori H, Yosikawa K, and Yazawa K.** Decreased heart rate by acupuncture stimulation in humans via facilitation of cardiac vagal activity and suppression of cardiac sympathetic nerve. *Neurosci Lett* 227: 165–168, 1997.
27. **Ohsawa H, Okada K, Nishijo K, and Sato Y.** Neural mechanism of depressor responses of arterial pressure elicited by acupuncture-like stimulation to a hindlimb in anesthetized rats. *J Auton Nerv Syst* 51: 27–35, 1995.
28. **Ohsawa H, Yamaguchi S, Ishimaru H, Shimura M, and Sato Y.** Neural mechanism of pupillary dilation elicited by electro-acupuncture stimulation in anesthetized rats. *J Auton Nerv Syst* 64: 101–106, 1997.
29. **Petty MA and Reid JL.** The effect of opiates on arterial baroreceptor reflex function in the rabbit. *Naunyn Schmiedebergs Arch Pharmacol* 319: 206–211, 1982.
30. **Richter A, Herlitz J, and Hjalmarson A.** Effect of acupuncture in patients with angina pectoris. *Eur Heart J* 12: 175–178, 1991.
31. **Sato T, Kawada T, Inagaki M, Shishido T, Takaki H, Sugimachi M, and Sunagawa K.** New analytic framework for understanding sympathetic baroreflex control of arterial pressure. *Am J Physiol Heart Circ Physiol* 276: H2251–H2261, 1999.
32. **Si QM, Wu GC, and Cao XD.** Effects of electroacupuncture on acute cerebral infarction. *Acupunct Electrother Res* 23: 117–124, 1998.
33. **Sved AF, Ito S, and Madden CJ.** Baroreflex dependent and independent roles of the caudal ventrolateral medulla in cardiovascular regulation. *Brain Res Bull* 51: 129–133, 2000.
34. **Tam KC and Yiu HH.** The effect of acupuncture on essential hypertension. *Am J Chin Med* 3: 369–375, 1975.
35. **Taneyama C, Goto H, Kohno N, Benson KT, Sasao J, and Arakawa K.** Effects of fentanyl, diazepam, and the combination of both on arterial baroreflex and sympathetic nerve activity in intact and baro-denervated dogs. *Anesth Analg* 77: 44–48, 1993.
36. **Tjen-A-Looi SC, Li P, and Longhurst JC.** Prolonged inhibition of rostral ventral lateral medullary premotor sympathetic neurons by electroacupuncture in cats. *Auton Neurosci* 106: 119–131, 2003.

37. **Tjen-A-Looi SC, Peng L, and Longhurst JC.** Medullary substrate and differential cardiovascular responses during stimulation of specific acupoints. *Am J Physiol Regul Integr Comp Physiol* 287: R852–R862, 2004.
38. **Wang JD, Kuo TB, and Yang CC.** An alternative method to enhance vagal activities and suppress sympathetic activities in humans. *Auton Neurosci* 100: 90–95, 2002.
39. **Wong AM, Leong CP, Su TY, Yu SW, Tsai WC, and Chen CP.** Clinical trial of acupuncture for patients with spinal cord injuries. *Am J Phys Med Rehabil* 82: 21–27, 2003.
40. **Wong AM, Su TY, Tang FT, Cheng PT, and Liaw MY.** Clinical trial of electrical acupuncture on hemiplegic stroke patients. *Am J Phys Med Rehabil* 78: 117–122, 1999.
41. **Yamamoto K, Kawada T, Kamiya A, Takaki H, Miyamoto T, Sugimachi M, and Sunagawa K.** Muscle mechanoreflex induces the pressor response by resetting the arterial baroreflex neural arc. *Am J Physiol Heart Circ Physiol* 286: H1382–H1388, 2004.
42. **Yao T.** Acupuncture and somatic nerve stimulation: mechanism underlying effects on cardiovascular and renal activities. *Scand J Rehabil Med Suppl* 29: 7–18, 1993.

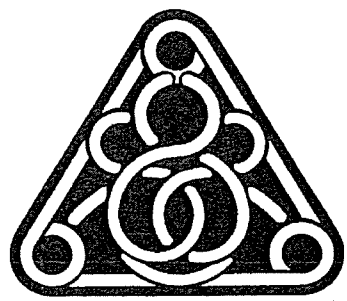

ELSEVIER

International Journal of Cardiology xx (2005) xxx – xxx

International Journal of Cardiology

www.elsevier.com/locate/ijcard

Postexercise VO_2 "Hump" phenomenon as an indicator for inducible myocardial ischemia in patients with acute anterior myocardial infarction

Hiroshi Takaki [a,*], Satoru Sakuragi [b], Noritoshi Nagaya [b], Shoji Suzuki [b], Yoichi Goto [b], Takayuki Sato [c], Kenji Sunagawa [a]

[a] *Department of Cardiovascular Dynamics, National Cardiovascular Center Research Institute, 5-7-1 Fujishiro-dai, Suita, Osaka, 565-8565, Japan*
[b] *Division of Cardiology, Department of Internal Medicine, National Cardiovascular Center, Suita, Japan*
[c] *Department of Cardiovascular Control, Kochi Medical School, Nankoku, Japan*

Received 13 October 2004; received in revised form 30 May 2005; accepted 24 July 2005

Abstract

Objectives: At exercise testing with respiratory gas analysis in patients with inducible myocardial ischemia, we have occasionally observed abnormal transient oxygen uptake (VO_2) components with a characteristic "Hump"-shaped morphology early after exercise, which may serve as an index for inducible ischemia. We examined this hypothesis in patients with anterior q-wave myocardial infarction in whom the accuracy to identify ischemia by exercise ECG is limited.

Design: From patients with acute anterior q-wave infarction but without clinically overt heart failure who underwent pre-discharge exercise testing, we examined patients with (Group-I, $n=30$) and without (Group-N, $n=29$) inducible ischemia. To identify "Hump", postexercise VO_2 (up to 4 min) standardized for peak VO_2 was exponentially fitted with use of peak VO_2 and VO_2 of 90–240 s, yielding "expected VO_2". "D-curve" was obtained by subtracting "expected VO_2" from measured VO_2.

Results: Although exercise-induced ST depressions more frequently appeared in Group-I (27%) than in Group-N (3%, $p<0.05$), the prevalence was low. D-curve peaked later ($p<0.01$) and its value was greater ($p<0.05$) in Group-I than in Group-N. When "Hump" was defined to be present if D-curve peaked ≥ 40 s and its peak value $\geq 15\%$, it was far more frequently found in Group-I ($n=17/30$) than in Group-N ($n=1/29$, $p<0.01$). Thus, "Hump" could diagnose inducible ischemia with a sensitivity of 57% and a specificity of 97%.

Conclusions: Although not highly sensitive, postexercise VO_2 "Hump" with its peak occurring around 60 s after exercise is a specific marker for inducible ischemia. The identification may be useful, particularly in patients with limited accuracy of exercise ECG such as those with q-wave anterior infarction.

Keywords: Exercise test; Respiratory gas analysis; Myocardial ischemia; Oxygen uptake

1. Introduction

In patients after acute myocardial infarction, the evaluation of inducible myocardial ischemia is important in the subsequent management, [1–3]] however, the diagnostic accuracy of exercise ECG is known to be limited in those patients [4–8]]. This is particularly crucial in patients with q-wave anterior infarction, in whom exercise-induced ST-segment depression would be often obscured by the presence of q-wave in the precordial leads.

Exercise testing with respiratory gas analysis is most often performed for evaluating the functional capacity and predicting prognosis in patients with heart failure, however, we have conducted the test in a considerable number of these post-infarct patients (approximately 200 tests/year) in our institute for more than 10 years [9]. Although the concomitant use of respiratory gas analysis is conducted mainly for the same purpose as above, postexercise oxygen uptake (VO_2) kinetics may provide useful information for detecting inducible ischemia in these patients. In practice,

* Corresponding author. Tel.: +81 6 6833 5012; fax: +81 6 6835 5403.
E-mail address: htakaki@res.ncvc.go.jp (H. Takaki).

0167-5273/$ - see front matter © 2005 Elsevier Ireland Ltd. All rights reserved.
doi:10.1016/j.ijcard.2005.07.012

we have occasionally observed abnormal components with a characteristic "Hump"-shaped morphology in the early portion of the postexercise VO_2 decay in some of patients with evidence of inducible ischemia. The mechanism is unclear, however, it is conceivable that this phenomenon may be caused by enhanced stroke volume following resolution of ischemia during exercise, that is presumably responsible for delayed recovery of postexercise systolic blood pressure in patients with ischemia [10–15].

Abnormal VO_2 kinetics after exercise has been reported in patients with heart failure due to left ventricular dysfunction [16–18]. However, to our knowledge, no studies have examined the significance of the abnormal VO_2 kinetics after exercise occurring in association with inducible ischemia. We thus examined the diagnostic utility of this phenomenon ("Hump") as an indicator for inducible ischemia in patients after acute anterior q-wave infarction without clinically overt heart failure.

2. Methods

2.1. Study population

From the consecutive inpatients with acute anterior q-wave myocardial infarction but without overt heart failure who underwent both pre-discharge exercise testing with respiratory gas analysis (within 3 weeks after the onset of infarction) and coronary angiography (approximately 4 weeks after the onset), we recruited the study population as follows. As a control group, we selected 29 patients (Group-N) who had no significant (>50% luminal diameter narrowing) stenosis in the coronary arteries at angiography, although 83% (n=24/29) of these patients had received percutaneous coronary intervention (PCI) during the acute phase of their infarction. It was assumed that this group did not have inducible ischemia. In 30 patients with abnormal coronary arteries, exercise thallium-201 scintigraphy (single-photon emission computed tomography; SPECT) showed reversible perfusion defects corresponding to the anatomic lesions demonstrated (Group-I). Of these patients, 43% (n=13/30) had received PCI during the acute phase, and at subsequent angiography 22 were left with single, five with double, and three with triple vessel disease (Table 1). All patients with Group-I subsequently received revascularization with either percutaneous transluminal angioplasty (n=26) or coronary artery bypass graft surgery (n=4).

We excluded patients with primary lung disease, orthopedic difficulties that precluded maximal exercise, arteriosclerotic obliterance and significant arrhythymias including atrial fibrillation. The patients with VO_2 plateau or leveling off (defined as an increase in VO_2 of less than 50 ml/min) around at peak exercise were also excluded (n=2), because the present study aimed to evaluate the significance of abnormal VO_2 kinetics ("Hump") only seen in the recovery period.

Table 1
Patients' characteristics

	Group-I (N=30)	Group-N (N=29)	p value
Sex (M/F)	26/4	22/7	NS
Age (years)	64±8	61±10	NS
LV EF (%)	39±7	43±9	NS
History of prior MI	7(23%)	2(7%)	NS
PCI therapy	13(43%)	24(83%)	<0.01
Coronary artery disease			
SVD	22(73%)	–	
DVD	5(17%)	–	
TVD	3(10%)	–	
Medication			
beta-blocker	13(43%)	6(21%)	NS
Ca antagonist	15(50%)	18(62%)	NS
Nitrate	21(70%)	10(34%)	<0.05
Digitalis	0 (0%)	2(7%)	NS

Values are expressed as mean±SD.
LVEF, left ventricular ejection fraction; MI, myocardial infarction; PCI, percutaneous coronary intervention; SVD, single vessel disease; DVD, double vessel disease; TVD, triple vessel disease.

Left ventricular ejection fraction (LVEF) was similar between the two groups (Table 1). There were no significant differences in sex, age, and history of prior myocardial infarction. The use of cardiovascular drugs was similar in the two groups except for nitrate, and it was neither altered nor withheld for the exercise test. All patients gave informed consent for the study.

2.2. Exercise testing

Symptom-limited exercise testing with respiratory gas analysis was performed on an upright bicycle ergometer in a ramp fashion. After a 2-min rest, exercise was begun with a 1-min warm up at 0 W at 60 rpm, followed by 15 W incremental loading every 1 min. ECGs (V_1, V_5, aV_F) and heart rate (HR) were monitored throughout the testing, while recording hardcopies of 12-lead ECG every 1 or 2 min. HR and blood pressure (BP) measured by a conventional cuff sphygmomanometer were recorded at rest, at 1-min intervals during exercise, and 1, 2, and 4 min into the recovery period. All patients stopped exercise because of dyspnea and/or leg fatigue, and there was no patient in whom exercise was stopped because of angina, marked ST-segment depressions or fall of blood pressure. Patients were asked to stop pedaling soon after exercise (up to 10 s) to avoid the possible influence of cool-down exercise on recovery VO_2 kinetics.

Expired gas was measured on a breath-by-breath basis at rest, during the exercise, and recovery period (at least up to 4 min) with a respiromonitor AE280 (Minato Medical Electronics, Osaka, Japan). The system was carefully calibrated before each study. VO_2, carbon dioxide production (VCO_2), and minute ventilation (VE) were stored in a computer hard disk every 6 s for later analysis.

We identified a significant ST-segment depression induced by exercise according to the following criteria; (1) a horizontal or downsloping ST-segment displacement at J-point $\geq$0.1 mV (2) up-sloping ST-segment displacement at 80 ms after the J-point $\geq$0.15 mV in at least 3 consecutive beats at peak exercise. A significant ST-segment elevation was defined as an upward shift of the ST-segment $\geq$0.1 mV at the J-point compared with the resting level.

2.3. Exercise SPECT

The test was performed with symptom-limited bicycle exercise. At near-maximal exercise, thallium-201 was intravenously injected and the patient was encouraged to exercise for another 1 min. SPECT images were obtained at 15 min (initial images) and 4 h (delayed images). The images were assessed by two experienced physicians unaware of the patient clinical information. Thallium uptake was classified as normal, mildly, moderately or severely reduced, or absent. A reversible defect was defined when the classification improved by at least one category from the initial to delayed image.

2.4. Data analysis

By using our custom-made software, we evaluated abnormal manifestations ("Hump") in early postexercise VO_2 decay (Fig. 1). To characterize "Hump", we performed the following procedures, assuming that postexercise VO_2 decay would normally (i.e., without inducible ischemia) follow an approximately exponential curve and that "Hump" would be expressed by the components that was not fitted by this approximation. We first standardized the time-series of VO_2 data following exercise up to 4 min for peak VO_2. The curve was monoexponentially fitted with use of peak VO_2 and continuous VO_2 data over the period of 90–240 s; i.e., the data from 6 to 90 s were excluded from the fitting because we had observed abnormal components in this period. Nonlinear least-squares fitting was made assuming a monoexponential model: $y=Z_0\times e^{-t/\mu}+Z_\infty$ (where y is the standardized VO_2 data, Z_0 is the initial standardized VO_2 above Z_∞, μ is the time constant, t is time after the termination of exercise and Z_∞ is the asymptote to which standardized VO_2 decay).

The fitted curve was termed the "expected VO_2 curve" in this study (Fig. 1). To characterize "Hump" phenomenon, we obtained the "D-curve" by subtracting the expected VO_2 curve from actually measured VO_2 curve. In the D-curve that was a function of time (every 6 s) after exercise, we determined the peak value (D_{max}) in amplitude and the elapsed time at the time point of D_{max} (T_{max}). These two indices were compared between the two groups.

Systolic BP and HR at rest, at peak exercise and at the recovery period of 1, 2, and 4 min after exercise were also analyzed.

2.5. Statistical analysis

Values are expressed as mean±SD. Between-group differences for unpaired values were analyzed by Student's t test and by the Mann–Whitney U test when appropriate. Repeated measures of analysis of variance were used to

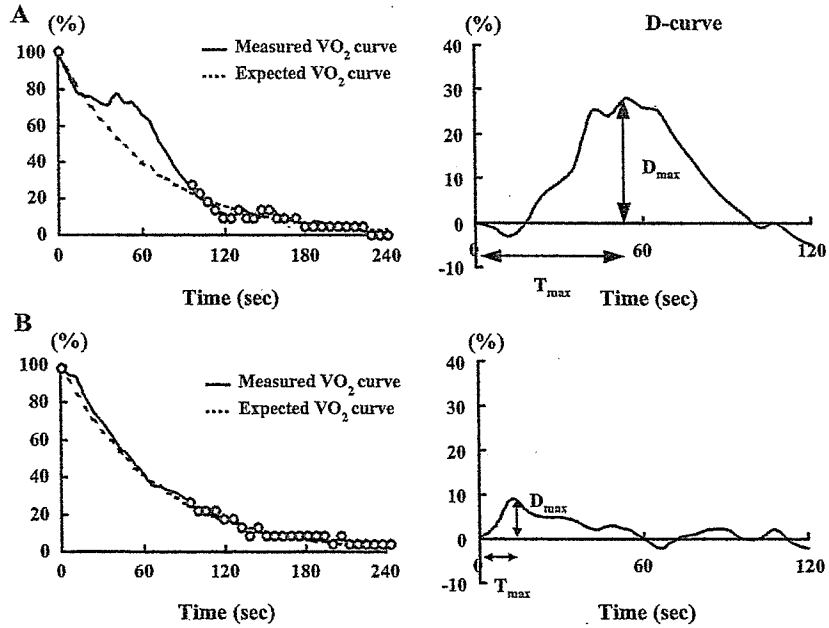

Fig. 1. Representative examples of postexercise VO_2 decay (left panel) and the derived D-curve (right panel) of two patients. Illustrated in the upper panels (A) are graphs for a patient of Group-I, and the lower (B) depict those for a patient of Group-N. After VO_2 decay curve standardized for peak VO_2 was exponentially fitted with use of peak VO_2 and VO_2 over the period of 90–240 s ("expected VO_2 curve", broken line), we obtained D-curve by subtracting "expected VO_2 curve" from actually measured VO_2 curve. In the D-curve, D_{max} (peak value) and T_{max} (time to peak) were estimated. VO_2=oxygen uptake.

Table 2
Exercise variables

	Group-I (N=30)	Group-N (N=29)	p-value
Rest HR (bpm)	70±12	75±17	NS
Rest SBP (mm Hg)	128±26	119±16	NS
Duration of exercise (s)	510±66	553±87	<0.05
Exercise-induced angina	3(10%)	0(0%)	NS
Peak HR (bpm)	137±27	147±24	NS
Peak SBP (mm Hg)	174±25	178±25	NS
ECG change			
ST elevation	14(47%)	16(55%)	NS
ST depression	8(27%)	1(3%)	<0.05
Peak WR (watt)	113±19	123±22	NS
Peak VO_2 (ml/min)	1179±192	1335±278	<0.05

Values are expressed as mean±SD. HR, heart rate; SBP, systolic blood pressure; VO_2, oxygen uptake; WR, work rate.

compare the values during recovery period. When this test was significant, the Newman–Keuls post hoc test was performed for multiple comparisons. Difference in categorical variables was analyzed by chi-square analysis. A p-value <0.05 was considered statistically significant. Receiver operating characteristics curves (ROC) were used to assess the ability of T_{max} and D_{max} to diagnose inducible ischemia [19].

3. Results

3.1. Exercise testing results

Table 2 shows exercise parameters for Group-I and Group-N. There were no significant differences in rest HR, rest systolic BP (SBP), peak HR or peak SBP between the two groups. Although peak work rate was similar between the two groups, the duration of exercise was shorter and peak VO_2 was lower in Group-I than Group-N ($p<0.05$, both). However, these 2 parameters were of little help for differentiating the two groups; for instance, there was considerable overlap in peak VO_2 between the groups. Only 3 patients of Group-I complained of anginal symptoms after exercise.

As for ECG parameters, the frequency of a significant exercise-induced ST-segment elevation was comparable between Group-I and Group-N (47% and 55%, respectively). Despite the presence of inducible ischemia, a significant ST-segment depression was found in only 8 of 30 patients (27%) in Group-I, although it was more frequently observed in Group-I than in Group-N (27% vs. 3%, $p<0.05$).

3.2. Comparison of postexercise VO_2

To evaluate the overall difference in postexercise VO_2 decay (D-curve) between the 2 groups, we averaged the value of D-curve over every 30 s in the first 2 min of the recovery period (Fig. 2, upper two panels). As a result, the magnitude was significantly greater in the period of 30–60 s than in the period of 0–30 s in Group-I (13.7%±8.2% vs. 8.7%±5.1%, $p<0.01$, Fig. 2A), whereas such a difference was not observed in Group-N (11.0%±5.2% vs. 10.2%±5.0%, NS, Fig. 2B).

To characterize the "Hump" phenomenon in D-curve, the peak value (D_{max}) and its elapsed time (T_{max}) were compared between the groups. T_{max} was significantly longer in Group-I than in Group-N (42.6±14.6 vs. 31.2±13.2 s,

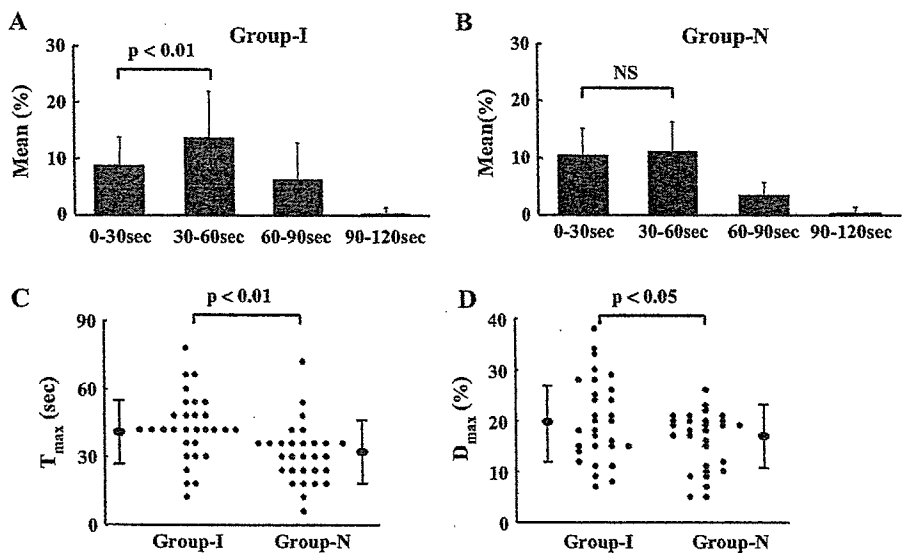

Fig. 2. The time-course changes in the D-curve for the first 2 min of recovery (upper panel) and comparisons of T_{max} (C, lower left panel) and D_{max} (D, lower right panel) between Group-I and Group-N. The D-curve values averaged over every 30 s were shown as bar graphs for Group-I (A, upper left panel) and Group-N (B, upper right panel). The mean for 30–60 s was greater than that for 0–30 s in Group-I ($p<0.01$), but not in Group-N. T_{max} was longer in Group-I than in Group-N ($p<0.01$), and D_{max} was greater in Group-I than in Group-N ($p<0.05$).

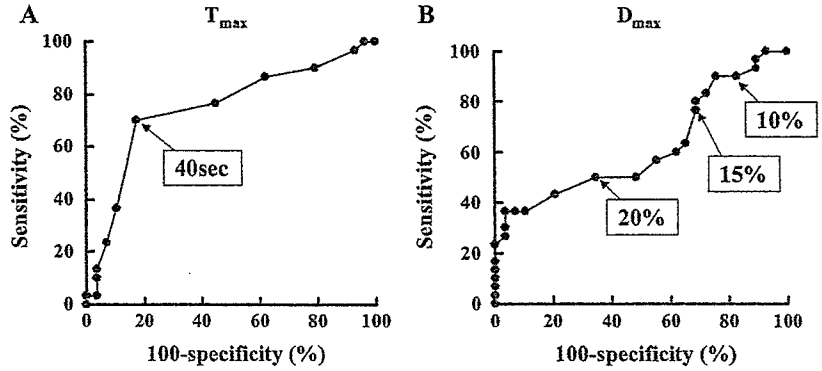

Fig. 3. ROC curves describing the ability for the diagnosis for inducible ischemia using T_{max} (A, left panel) and D_{max} (B, right panel).

$p<0.01$, Fig. 2C), and D_{max} was also significantly greater in Group-I than in Group-N (20.1%±8.1% vs. 16.2%±5.7%, $p<0.05$, Fig. 2D).

We used ROC analysis to determine the optimum cutoff values of these two parameters for identifying Hump phenomenon, i.e., inducible ischemia. When ROC analysis was conducted separately for T_{max} (Fig. 3A) and D_{max} (Fig. 3B), we could easily recognize 40 s as the optimum cutoff for T_{max} in differentiating the two groups, whereas such an optimum point was not found for D_{max}. Since it is considered that the combination of the two optimum cutoff values, each of which was determined by a separate ROC analysis, would not necessarily have the highest discriminative power, ROC analysis of T_{max} was repeated for a given D_{max}, while shifting D_{max} every 1% from 0% to 40%. As a result, when assuming that the best cutoff was defined as the point with highest sum of sensitivity and specificity, the combination of $D_{max} \geq 10\%$ and $T_{max} \geq 40$ s (from 37 to 41 s, because temporal resolution was 6 s) could most accurately discriminate Group-I from Group-N (sensitivity 67%, specificity 90%, accuracy 78%, Table 3). When $D_{max} \geq 15\%$ was applied (Fig. 4), the specificity was increased to 97%, although the sensitivity decreased to 57%.

3.3. Comparison of postexercise SBP

Although resting and peak SBP were not different between the two groups, Group-I had a higher SBP than Group-N at 2 and 4 min of recovery (both $p<0.05$, Fig. 5A).

Furthermore, among patients of Group-I, patients with "Hump", defined as $T_{max} \geq 40$ s and $D_{max} \geq 15\%$, had a higher SBP at 1 and 2 min of recovery than those without "Hump" (both $p<0.05$, Fig. 5B). A significant decrease in SBP from peak exercise was found at 1 min of recovery in patients without "Hump", but not in those with "Hump".

Table 3
Diagnostic accuracy of "Hump" for identifying inducible ischemia (Group-I)

T_{max} (s)	≥40	≥40	≥40
D_{max} (%)	≥10	≥15	≥20
Sensitivity	67% (20/30)	57% (17/30)	37% (11/30)
Specificity	90% (26/29)	97% (28/29)	100% (29/29)
Accuracy	78%	76%	68%

4. Discussion

Although exercise-induced ST-segment depression is a cardinal index to identify inducible myocardial ischemia on exercise testing, the diagnostic accuracy by the standard ST criteria is limited in post-infarct patients [4–8]. In our population consisting of patients after acute anterior q-wave myocardial infarction, ST-segment depressions during exercise appeared in only 27% of patients with inducible myocardial ischemia (Group-I), that was comparable to the incidence of ST depression reported previously [6–8]. The most likely explanation for the low sensitivity of ST depression in these patients is that exercise-induced ST elevation over q-wave leads, related to left ventricular asynergy, would mask the appearance of ST depression [5,20]. In patients with anterior q-wave myocardial infarction, the vector of ST-segment depression, which most frequently appears in the left precordial leads of V_4 to V_6,

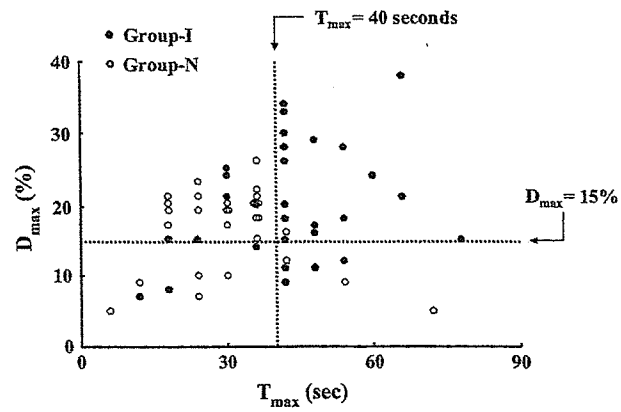

Fig. 4. Scatterplots showing D_{max} plotted against T_{max} for each patient. Approximately half (57%) of patients of Group-I (closed circle) were distributed in the limited area of $T_{max} \geq 40$ s and $D_{max} \geq 15\%$, whereas only one patient in Group-I (open circle) was distributed in this area. Using this criterion, we could diagnose the presence of inducible ischemia (Group-I) with a sensitivity of 57% and a specificity of 97%.

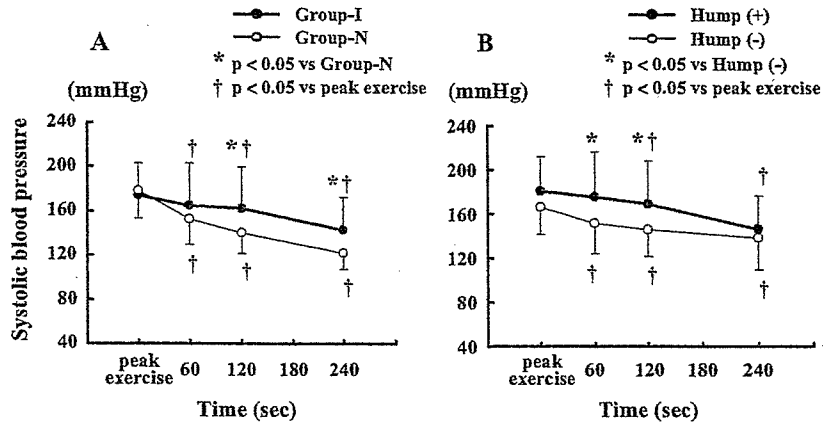

Fig. 5. Comparisons of systolic blood pressure time-course after exercise between Group-I and Group-N (A, left panel), and between the Group-I patients with and without "Hump" phenomenon (B, right panel).

may be electrically canceled by the opposite vector of ST elevation occurring in association with ventricular asynergy.

It is generally accepted that exercise-induced ST-segment elevation over post-infarct q-wave leads occurs in association with severe left ventricular asynergy, however, several studies indicated that exercise-induced ST-segment elevation might occur due to induced ischemia [21,22]. In the present study, we observed a similar prevalence of ST-segment elevation of ≥ 0.1 mV in Group-N (55%) and Group-I (47%, NS), suggesting that this index alone is of no use for identifying ischemia. We cannot exclude the possibility that ST-segment elevation might be caused by ischemia in some patients of Group-I, because three Group-I patients presented both exercise-induced ST-segment elevation and depression.

On the other hand, the present study has shown that abnormal transient VO_2 components after exercise, "Hump" phenomenon defined by our method described above, is a useful indicator for inducible ischemia in patients with acute anterior infarction. When the combination of $T_{max} \geq 40$ s and $D_{max} \geq 15\%$ were used for the definition of "Hump", we could diagnose inducible ischemia with sensitivity of 57%, specificity of 97%.

Abnormal postexercise VO_2 kinetics has been reported previously in patients with cardiocirculatory disorders. Hayasida et al. and other authors reported that the recovery of VO_2 was prolonged in patients with left ventricular dysfunction and that the time-course of VO_2 decay after exercise was closely related to exercise capacity [16–18,23–27] and prognosis [28]. Delayed energy store recovery in the skeletal muscle [22,24] and prolonged decrease in cardiac output [23,25–27,29] are considered to be involved in the genesis of this abnormal VO_2 recovery.

To our knowledge, there have been no published studies specifically examining the significance of exercise-induced ischemia on the postexercise abnormal VO_2 kinetics. Abnormal components of our interest, i.e., "Hump", is characterized by a transient convex bulge in the limited portion of VO_2 decay at around 1 min. The occurrence seems to appear not immediately but soon after the termination of exercise, generally lasting approximately 1 min. Previous reports estimated abnormal VO_2 kinetics by estimating the whole VO_2 decay with use of temporal parameters such as half time, [18,24,26] time constant [16,23,25] or cumulative area [28]. Since these measures are clearly unsuitable for our purpose, the non-exponential components (i.e., D-curve), that were derived by subtraction assuming that the abnormal components would be superimposed upon the monoexponential VO_2 decay, were compared between Group-I and Group-N. As a result, in Group-I, the mean value averaged over 30–60 s was greater than that averaged over 0–30 s, whereas such a difference was not found in Group-N (Fig. 2, upper two panels). Furthermore, the D-curve peaked later and its maximal value was greater in Group-I compared with Group-N (Fig. 2, lower two panels). Thus, the group difference of the D-curve with respect to the amplitude and temporal profile enabled us to identify the presence of inducible ischemia by the criterion shown in Table 3.

It was somewhat unexpected that some of patients without inducible ischemia (Group-N) showed a sizable amount of non-exponential components in the very early period of recovery up to 30 to 40 s. Our expectation was that non-exponential components in Group-N would be negligibly small, because the VO_2 decay curve should be closely fitted by the monoexponential model. This discrepancy indicates that postexercise VO_2 decay is not necessarily monoexponential in shape, and may be more precisely fitted by other mathematical models such as a sigmoidal model, even in the absence of inducible ischemia, although simple noise inherent in the measurements might be also related to the components. Impairment of LV function due to infarction and peripheral dysfunction caused by the immobilization (deconditioning effects) in the acute phase of myocardial infarction would contribute to the loss of the rapid fall of VO_2 immediately after exercise.

Several studies indicated that, in patients with inducible myocardial ischemia, an abnormal systolic blood pressure